

Topological Freeze-out by Semi-Annihilation

Joe Davighi,^a Serah Moldovsky,^{b,c} Hitoshi Murayama,^{b,c,d,1} Christiane Scherb,^{b,c}
Nudžeim Selimović^e

^a*Theoretical Physics Department, CERN, 1211 Geneva 23, Switzerland*

^b*Department of Physics, University of California, Berkeley, CA 94720, USA*

^c*Ernest Orlando Lawrence Berkeley National Laboratory, Berkeley, CA 94720, USA*

^d*Kavli Institute for the Physics and Mathematics of the Universe (WPI), University of Tokyo Institutes for Advanced Study, University of Tokyo, Kashiwa 277-8583, Japan*

^e*Istituto Nazionale di Fisica Nucleare, Sezione di Padova, Via Francesco Marzolo 8, 35131 Padova, Italy*

E-mail: joseph.davighi@cern.ch, serah.moldovsky@berkeley.edu,
hitoshi@berkeley.edu, cscherb@lbl.gov, nudzeim.selimovic@pd.infn.it

ABSTRACT: We point out that a QCD-like dark sector can be coupled to the Standard Model by gauging the topological Skyrme current, which measures the dark baryon number in the infrared, to give a technically natural model for dark matter. This coupling allows for a semi-annihilation process $\chi\chi \rightarrow \chi X_\mu$, where X_μ is the gauge boson mediator and χ a dark pion field, which plays the dominant role in setting the dark matter relic abundance. The topological interaction is purely p -wave and so free from indirect detection constraints. We show that the dark matter pion mass needs to be in the range $10 \text{ MeV} \lesssim m_\chi \lesssim 1 \text{ TeV}$; towards the lighter end of this range, there can moreover be significant self-interactions. We discuss prospects for probing this scenario at collider experiments, ranging from the LHC to low-energy e^+e^- colliders, future Higgs factories, and beam-dump experiments.

¹Hamamatsu Professor

Contents

1	Introduction	2
2	The Model	4
2.1	't Hooft Naturalness and Dark Pion Stability	5
2.2	Generalised Symmetry Matching	5
3	Dark Sector Processes	7
3.1	Semi-Annihilation Channel	7
3.2	Annihilation Channel	8
3.2.1	NDA Estimate	9
3.2.2	IR Estimate	9
3.2.3	UV Estimate	10
3.2.4	Annihilation Cross-Section	10
3.3	Kinetic Equilibrium	11
3.4	Self-Heating	13
4	Boltzmann Equation	13
4.1	Semi-Annihilation Contribution	14
4.2	Full Contribution	16
4.3	Parameter Space	17
5	Phenomenology	19
5.1	Direct and Indirect Detection	19
5.2	Dark Photon Bounds	19
5.3	Collider Phenomenology	20
6	Conclusion and Outlook	23
A	Semi-Annihilation Computations	24
B	Annihilation Computations	26
C	Semi-Analytical <i>vs.</i> Numerical Results	27

1 Introduction

Understanding the nature of dark matter (DM), and how it interacts with Standard Model (SM) particles, are central challenges in fundamental physics [1]. The absence of any clear experimental clues coming from (in)direct detection or collider experiments motivates us to look beyond the most simple models for DM. And given the rich structure we observe in the visible sector, wherein the stable electron and proton are accompanied by a zoo of unstable particles, a compelling scenario is that DM comprises a few stable particles belonging to some similarly rich dark sector (DS). One appealing possibility is that of a confining QCD-like dark sector [2], say a dark $SU(N_c)$ gauge group acting on N_f dark quarks Q_i in the fundamental representation. For suitably chosen N_c and N_f , we expect the infrared (IR) dynamics to be governed by a chiral symmetry breaking transition that delivers weakly-interacting pions χ^a , some of which can be stable [3] and thus DM candidates.

Of course, once we go down this road we open up a Pandora’s box of possible DS theories. It is pragmatic to focus on the different *portals* through which the DS can communicate with the SM, of the form $\mathcal{L} = \mathcal{O}_{\text{SM}}\mathcal{O}_{\text{DS}}$. Such a portal interaction (i) enables thermalisation of the DM with the SM, and so determines the relic abundance *e.g.* via freeze-out, and (ii) provides channels through which DM might be produced today in experiment. For example the vector portal [4], by which a dark photon X_μ talks to the SM through kinetic mixing with the photon, is one of only three renormalisable portal interactions [5, 6].

Given the hypothesis of a confining QCD-like sector, perhaps the most natural way to couple it to the SM is to gauge the dark baryon number current $j_{B,\text{UV}}^\mu = \frac{1}{N_c} \sum_i \bar{Q}_i \gamma^\mu Q_i$, which is an anomaly-free global symmetry of the DS, then couple to the SM via the vector portal, *viz.*

$$\mathcal{L}_{\text{portal,UV}} = e_B X_\mu j_{B,\text{UV}}^\mu - \frac{\epsilon}{2} X_{\mu\nu} F^{\mu\nu} \quad (1.1)$$

where $X_{\mu\nu} = \partial_{[\mu} X_{\nu]}$ is the dark baryon field strength and $F_{\mu\nu} = \partial_{[\mu} A_{\nu]}$ is the photon field strength. Somewhat surprisingly, this simple possibility has been largely overlooked, and is the subject of this paper. We find its low-energy phenomenology has many striking features.

The key realisation is an old one: namely that, upon flowing to the IR, baryon number in a confining $SU(N_c)$ gauge theory can be identified with the topological winding number measuring the homotopy class of the pion field configuration [7–10], that is an element in $\pi_3(SU(N_f)_L \times SU(N_f)_R / SU(N_f)_V) \cong \mathbb{Z}$. This is obtained by integrating the current

$$j_{B,\text{IR}}^\mu = \frac{1}{24\pi^2} \epsilon^{\mu\nu\rho\sigma} \text{Tr} (U^{-1} \partial_\nu U U^{-1} \partial_\rho U U^{-1} \partial_\sigma U) , \quad (1.2)$$

where $U(x) = e^{2i\chi^a(x)t^a/f_\pi}$ is the $SU(N_f)$ -valued dark pion field, with f_χ being the corresponding decay constant. The portal coupling in (1.1) therefore becomes a *topological interaction* in the IR, that is, loosely speaking, a term in the action that is obtained by directly integrating a differential form,¹ similar to the Wess–Zumino–Witten (WZW) term in QCD [15, 16].

¹In the context of dark sector theories, topological interactions have previously been used (i) to realise the

Locally, *i.e.* for small field values, we can write the Lagrangian

$$\mathcal{L}_{\text{portal,IR}} = \frac{e_B}{12\pi^2 f_\chi^3} \epsilon^{\mu\nu\rho\sigma} f_{abc} X_\mu \partial_\nu \chi^a \partial_\rho \chi^b \partial_\sigma \chi^c - \frac{\epsilon}{2} X_{\mu\nu} F^{\mu\nu} + O(\chi^4), \quad (1.3)$$

where f_{abc} are the structure constants for $SU(N_f)$. Thus the dark pions χ^a , which we expect to be stable and thus serve as our DM candidate, talk to the SM via a 4-point interaction involving three pions and one gauge boson.

We land on a DS theory in which dark pions talk to the vector X , which is itself thermalised with the SM through the vector portal, through a $2 \rightarrow 1$ number-changing process. An interaction of this kind, $\chi\chi \rightarrow \chi X$, can realise the DM thermal freeze-out scenario known as ‘semi-annihilation’ [17]. There is no need to impose *ad hoc* \mathbb{Z}_3 global symmetries to dictate this $2 \rightarrow 1$ interaction structure; here it follows unavoidably from the fact that, given we seem to live in a three-dimensional space, a topological current corresponds to an invariant, closed differential 3-form. Moreover, there is no contribution to the elastic channel $\chi\chi XX$ arising at tree-level, since the gauge field X_μ (and hence A_μ) talks to the dark sector purely through the abelian gauge interaction whose structure is fixed to be linear in X_μ . Operators inducing $\chi\chi XX$ transitions are expected to arise at 1-loop, originating from a dark quark box diagram in the UV theory which we estimate below, and so are subleading with respect to the $\chi\chi\chi X$ channel. Our simple setup, namely dark QCD with gauged baryon number, therefore provides a natural UV completion for semi-annihilation.²

In addition to being able to fit the observed DM relic abundance through thermal freeze-out,³ the composite nature of dark matter allows for a significant velocity-dependent self-interaction amongst the dark pions, that offers a possible explanation [20–22] of various small scale structure puzzles regarding galaxy formation [23–30] – sometimes known as the ‘core-cusp problem’ or the ‘diversity problem.’

Another striking feature of this model is that, because the interaction is topological and thus equipped with three derivatives acting on the dark pion fields (1.3), the semi-annihilation process is necessarily p -wave. Without any tuning, this framework therefore evades otherwise strong constraints that would come from cosmic microwave background (CMB) observations [31], and indirect detection constraints due to gamma-ray emission from the galactic center [32]. This allows the DM mass to be light, into the sub-GeV range.

In this paper we explore the phenomenology of this elegant DS realisation of freeze-out by semi-annihilation, through the topological interaction (1.3) obtained by gauging baryon number. We numerically solve the Boltzmann equations, including both the tree-level $\chi\chi \leftrightarrow$

strongly interacting massive particle (SIMP) DM paradigm [11] (by achieving $3 \rightarrow 2$ conversion within a sector of dark pions through the WZW term [12]), and (ii) to form a direct ‘topological portal’ that converts QCD pions (and $\pi^0\gamma$) to a pair of dark pions living on $SU(2)/SO(2) \cong S^2$ [13, 14].

²Another natural UV completion for semi-annihilation exploits the structure of the Yang–Mills interaction, namely that there are cubic interactions between gauge bosons. Including also a charged scalar that talks to the SM via the scalar portal gives rise to the ‘hidden vector dark matter’ model [18].

³The same type of vertex can also lead to an exponential growth in the dark matter abundance through freeze-in [19], which allows for a very heavy dark matter.

χX semi-annihilation process and our estimate of the 1-loop induced $\chi\chi \leftrightarrow XX$, to obtain the region of parameter space for which the dark pions compose the whole DM relic abundance. This depends on the dark QCD parameters m_χ , f_χ , as well as the gauge coupling e_B that activates the portal to the SM. Interestingly, we find viable parameter space where, in addition to fitting relic abundance through semi-annihilation, the following are all satisfied: (i) $m_\chi < 4\pi f_\chi$ for EFT validity; (ii) m_χ and m_X are not so light as to modify N_{eff} at the time of Big Bang nucleosynthesis (BBN); and (iii) the self-interactions are within the limits from astrophysical observations. At the edge of the range, these self-interactions can be large enough to address the issues with small-scale structure.

We conclude by surveying the prospects for probing this scenario in various collider experiments, for instance through classic mono-photon and mono-jet searches but also through more exotic dark shower signatures. These collider probes take on a greater importance given that direct and indirect detection probes are nullified by the p -wave nature of the interaction.

The rest of the paper is structured as follows. In §2 we set out the main features of the topological freeze-out model. In §3 we compute the thermally-averaged cross-section for the semi-annihilation process, as induced at tree-level by the topological interaction, and also estimate the loop-induced annihilation channel. With these ingredients, we turn to solving the Boltzmann equations relevant for this dark matter model in §4, providing both numerical and semi-analytical solutions (which are in good agreement). We discuss collider phenomenology in §5, before concluding in §6.

2 The Model

Our model for the Dark Sector (DS) is simple: we posit an $SU(N_c)$ gauge theory with N_f flavours of Dirac fermion Q_i charged in the fundamental representation, with $U(1)_B$, the dark baryon number, also gauged. The Lagrangian reads

$$\mathcal{L}_{\text{UV}} = \mathcal{L}_{\text{SM}} - \frac{1}{2} \text{tr} G_{\mu\nu} G^{\mu\nu} - \frac{1}{4} X_{\mu\nu} X^{\mu\nu} - m_X^2 X_\mu X^\mu + \sum_i \bar{Q}_i (i\not{D} - m_Q) Q_i - \frac{\epsilon}{2 \cos \theta_w} X_{\mu\nu} B^{\mu\nu}, \quad (2.1)$$

where $D_\mu = \partial_\mu - igG_\mu - ie_B X_\mu$, with G_μ the dark $SU(N_c)$ gauge field and X_μ that of $U(1)_B$; here we write the kinetic mixing in a way that is valid above the electroweak scale, with $B_{\mu\nu}$ being the hypercharge field strength and θ_w the weak mixing angle. We assume there are at least two flavours $N_f \geq 2$ of dark quark Q_i , with a degenerate mass m_Q that is smaller than the dynamical scale of $SU(N_c)$, $m_Q < \Lambda_{N_c}$. Then below the strong scale the dark quarks are bound into pseudoscalar mesons χ^a , which we generically refer to as ‘(dark) pions’ and which serve as the dark matter in this model. For simplicity, we assume $N_f = 2$ for much of the discussion below. We include also a mass term for the dark photon, which could arise via the Higgs mechanism after spontaneously breaking $U(1)_B$ at a scale $\sim m_X/e_B$, or via the Stückelberg trick.

It might be surprising that the $U(1)_B$ gauge symmetry has anything to do with the dark pions because they do not carry baryon number. Yet, as we described in the Introduction, it was pointed out in [8] and later developed in [9, 10] that the low-energy baryon number current is given by

$$j_B^\mu = \frac{1}{24\pi^2} \epsilon^{\mu\nu\rho\sigma} \text{tr}(U^{-1}\partial_\nu U)(U^{-1}\partial_\rho U)(U^{-1}\partial_\sigma U), \quad (2.2)$$

as per (1.2). Thus, adding the gauge interaction $e_B X_\mu j_B^\mu$ to the standard chiral Lagrangian

$$\mathcal{L}_\chi = \frac{f_\chi^2}{4} \text{tr} \partial^\mu U^\dagger \partial_\mu U + \mu^3 m_Q (\text{tr} U + c.c.), \quad U(x) = e^{2i\chi^a(x)t^a/f_\chi}, \quad (2.3)$$

where $\mu^3 = \langle \bar{Q}Q \rangle$, and expanding it to the lowest order in χ^a , we obtain

$$\mathcal{L}_\chi = \frac{1}{2} (\partial^\mu \chi^a \partial_\mu \chi^a) - \frac{1}{2} m_\chi^2 \chi^a \chi^a + \frac{e_B}{12\pi^2 f_\chi^3} \epsilon^{\mu\nu\rho\sigma} f^{abc} X_\mu \partial_\nu \chi^a \partial_\rho \chi^b \partial_\sigma \chi^c + O(\chi^4). \quad (2.4)$$

The last term is a topological $\chi\chi\chi X$ vertex and causes semi-annihilation. Because we restrict to the case $N_f = 2$, the model does not feature the more familiar WZW topological term involving five dark pion fields. It would be interesting to relax this assumption in future work.

2.1 't Hooft Naturalness and Dark Pion Stability

The model is technically natural in the sense of 't Hooft [33]. There are no elementary scalars to cause a hierarchy problem. The assumption $m_Q < \Lambda_{N_c}$ is natural given that the limit $m_Q \rightarrow 0$ results in an enhancement of the symmetry, namely full chiral symmetry. The degeneracy among quarks can be ensured by a global flavour symmetry. Note that this degeneracy is important in order to ensure stability of the dark matter pions. For instance, the neutral dark pion $\chi^3 = (Q_1 \bar{Q}_1 - Q_2 \bar{Q}_2)/\sqrt{2}$ is stable because the triangle diagrams involving up-quark and down-quark cancel precisely as long as $m_{Q_1} = m_{Q_2}$. If they are not degenerate, the difference between them lets χ^3 decay into XX if $m_X < m_\chi/2$, or off-shell into Xe^+e^- etc if $m_\chi/2 < m_X < m_\chi$. If we are concerned that quantum gravity effects do not allow for a global flavour symmetry (see *e.g.* [34] and references therein), it can be an $SU(N_f = 2)$ gauge symmetry with small coupling $g \lesssim (8\pi m_\chi/M_{\text{Pl}})^{1/4} \sim 10^{-5} (m_\chi/100 \text{ MeV})^{1/4}$ to avoid the gauge bosons to be populated in the thermal bath, or it can be a discrete gauge symmetry such as S_3 where (u, d) is an irreducible doublet representation (see, *e.g.*, [35]).

2.2 Generalised Symmetry Matching

Before we proceed to elucidate the phenomenological consequences of this DS portal, we pause to highlight more formal aspects of its construction. More phenomenologically-minded readers may wish to skip ahead to §3. In this Subsection, we briefly entertain the more general possibility of an arbitrary number N_f of dark quark flavours.

Topological interactions in chiral Lagrangians play a key role when it comes to understanding the (possibly anomalous) symmetry structure of the theory in the infrared phase.

By integrating by parts, the local Lagrangian expression for the $\chi\chi\chi X$ term in (2.4) can be written in a manifestly gauge-invariant way, that is in terms of the field strength $X_{\mu\nu}$ rather than X_μ , as $\mathcal{L} \sim \epsilon^{\mu\nu\rho\sigma} \chi^a \partial_\mu \chi^b \partial_\nu \chi^c X_{\rho\sigma}$; but this Lagrangian is no longer manifestly invariant under the global flavour symmetry $SU(N_f)_L \times SU(N_f)_R$ which shifts the pion fields. This mirrors the story for the more familiar WZW term that also appears in our dark sector; in both cases, this quasi-invariance is strictly governed by the anomaly/symmetry structure of the underlying UV theory, which in turn governs why both topological interactions have quantised coefficients (in appropriate units).

To understand how this works for the less-familiar portal interaction, first note that both topological actions can be written in a manifestly invariant form at the expense of locality, *i.e.* by passing to one higher dimension and writing the action as an integral of a differential form over an open 5-manifold Y whose boundary is the 4-dimensional spacetime $\Sigma = \partial Y$ à la Witten [16]. Using the language of differential forms, we have

$$S_{\text{top}}[\Sigma = \partial Y] = \int_Y \frac{-iN_c}{480\pi^3} \text{Tr}(U^{-1}dU)^5 + \int_Y \frac{1}{24\pi^2} \text{Tr}(U^{-1}dU)^3 \wedge X, \quad (2.5)$$

where here $X := \frac{1}{2}X_{\mu\nu}dx^\mu \wedge dx^\nu$ is the field strength 2-form for the $U(1)_B$ gauge field, and where we have temporarily absorbed the pre-factor of e_B by redefining the gauge kinetic term in (2.1). The presence of a dynamical abelian gauge field bestows our DS with a 1-form global symmetry [36] $H^{[1]} = U(1)$, whose current is simply $j^{(2)} = X$, which is a closed 2-form. The objects charged under this 1-form symmetry are 't Hooft lines for X_μ . Furthermore, the second topological interaction in (2.5), which is the focus of this work, intertwines this 1-form symmetry with the $G^{[0]} = SU(N_f)_L \times SU(N_f)_R$ flavour symmetry to form what is known as a *2-group global symmetry* [37–39]. The same structure was recently observed for a closely related theory in [14].

While a detailed explanation is somewhat tangential to this work, a quick way to see this is to turn on minimally-coupled background fields for both $G^{[0]}$ and $H^{[1]}$, denoted $A_{L,R}^{(1)}$ and $B^{(2)}$ respectively. Then observe that the gauged action $S \supset \int_Y \frac{1}{8\pi^2} \text{Tr} [A_L dA_L + \frac{2}{3} A_L^3 - (L \leftrightarrow R)] \wedge X + i \int_\Sigma X \wedge B^{(2)}$ is invariant under the flavour background gauge transformations $A_{L,R} \rightarrow A_{L,R} + D_{A_{L,R}} \lambda_{L,R}^{(0)}$ iff the 2-form gauge field shifts as $B^{(2)} \rightarrow B^{(2)} + d\Lambda^{(1)} + \frac{1}{4\pi} \text{Tr}(\lambda_L^{(0)} dA_L - \lambda_R^{(0)} dA_R)$. This results in a modification of the Ward identities for the ordinary flavour symmetry currents $j_{L,R}^a$, even with the background gauge fields switched off [14, 38]. In the UV theory of dark QCD, this generalised symmetry structure arises as a consequence of a non-vanishing triangle diagram involving 2 flavour legs and 1 abelian gauge leg.

The upshot is that, while the ordinary WZW term matches a 't Hooft anomaly in the underlying theory (noting that our DS does not have the analogue of QED being gauged, so it is not in this case an ABJ anomaly), the second topological interaction, which is obtained by gauging the dark baryon number, matches a generalised 2-group symmetry, as in [14]. Indeed, the need to match this generalised symmetry in the infrared can be seen as a rigorous justification for the baryon number current being identified with the topological winding number in the first place. Both the anomaly coefficient and the 2-group coefficient are RG

invariants of the theory; equivalently, the couplings of the two topological interactions are quantised. The EFT matching onto these coefficients is leading-order exact, and can be computed in the weakly-coupled UV phase – unlike other non-topological interactions in the chiral Lagrangian.

At this point, we fix $N_f = 2$ again for the remainder of the paper – meaning, in particular, that the first term on the RHS of Eq. (2.5) is not present in our setup.

3 Dark Sector Processes

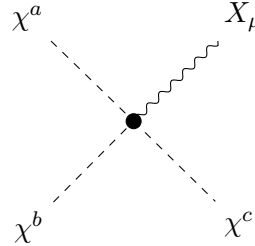
In this Section, we discuss important processes in the dark sector that will govern the evolution of both dark and visible species in the early Universe. These are (i) semi-annihilation $\chi\chi \rightarrow \chi X$ (§3.1), (ii) annihilation $\chi\chi \rightarrow XX$ (§3.2), (iii) thermalisation $X\chi \rightarrow X\chi$ (§3.3), and (iv) self-heating (§3.4). In order to discuss (ii) and (iii), we need to estimate the size of the effective $\chi\chi XX$ interaction which we do in §3.2.1.

3.1 Semi-Annihilation Channel

The chiral Lagrangian with a gauged $U(1)_B$ symmetry, given in Eq. (2.4), gives rise to the semi-annihilation process $\chi\chi \rightarrow \chi X$ thanks to the topological interaction in (2.4). Here we analyze this process quantitatively, and identify the region of parameter space in which the dark pions can account for the observed dark matter abundance.

The key quantity to compute is the thermally averaged cross-section, $\langle\sigma v\rangle_{\chi\chi\rightarrow\chi X}$, which determines the effective rate of the semi-annihilation process entering the Boltzmann equation for dark pions and, consequently, governs their relic abundance. Our goal is to determine whether there exists a region of parameter space in which the dark pions can constitute all the DM as a thermal relic, undergoing freeze-out via semi-annihilations with the dark photon.

Starting from the Lagrangian (2.4), the contact interaction involving three dark pions and one dark photon gives rise to the following Feynman rule



$$\sim -\frac{e_B}{2\pi^2 f_\chi^3} f^{abc} \epsilon^{\mu\nu\rho\sigma} p_{1\nu} p_{2\rho} p_{3\sigma}, \quad (3.1)$$

where $p_{1,2,3}$ denote the (all incoming) momenta of the pions. This can be used to construct the corresponding matrix element, and thence the cross-section upon performing the final-state phase-space integration

$$\sigma_{\chi\chi\rightarrow\chi X} = \frac{N_f}{N_f^2 - 1} \frac{e_B^2}{1536\pi^5} \frac{s^2}{f_\chi^6} \left(1 - \frac{m_\chi^2}{s}\right)^3 \left(1 - \frac{4m_\chi^2}{s}\right)^{1/2}, \quad (3.2)$$

where s is the center-of-mass energy of the $\chi\chi \rightarrow \chi X$ process. The details of this calculation are presented in App. A. Following Refs. [40, 41], we compute the thermally averaged cross section times the Møller velocity, $v = \sqrt{|\mathbf{v}_1 - \mathbf{v}_2|^2 - |\mathbf{v}_1 \times \mathbf{v}_2|^2}$, as the following integral

$$\langle \sigma v \rangle_{\chi\chi \rightarrow \chi X} = \frac{\int_{4m_\chi^2}^{\infty} \sigma_{\chi\chi \rightarrow \chi X} \sqrt{s}(s - 4m_\chi^2) K_1(\sqrt{s}/T) ds}{8m_\chi^4 T K_2^2(m_\chi/T)}, \quad (3.3)$$

with K_i being the modified Bessel functions of the i -th order. The result can be expressed in terms of Meijer-G functions [42], and we give such expressions in App. A for completeness.

Because the dark pions are nearly non-relativistic at the time of freeze-out, it is useful to Taylor expand the thermally averaged cross-section $\langle \sigma v \rangle_{\chi\chi \rightarrow \chi X}$ in inverse powers of $x := m_\chi/T$. We obtain

$$\langle \sigma v \rangle_{\chi\chi \rightarrow \chi X} = \frac{N_f}{N_f^2 - 1} \frac{e_B^2}{384\pi^5} \frac{m_\chi^4}{f_\chi^6} \left(\frac{81}{16} x^{-1} + \frac{891}{32} x^{-2} + \mathcal{O}(x^{-3}) \right). \quad (3.4)$$

We will use this expression as input to the Boltzmann equation in §4. There we will moreover show that the leading order term, proportional to x^{-1} in Eq. (3.4), captures the dominant contribution to the semi-annihilation rate, with deviations at the level of $\mathcal{O}(10\%)$ compared to the full numerical evaluation of Eq. (A.11) (from the Appendix).

The fact that the leading term in this expansion starts at order x^{-1} means that the semi-annihilation process at threshold is purely p -wave. This can be understood straightforwardly in the case where the final state dark photon is transverse, with helicity ± 1 , simply because of angular momentum conservation: namely, there is one unit of net angular momentum flowing along the axis of the final state χX system, and hence the total angular momentum must be at least one unit, while the initial state $\chi\chi$ system has angular momentum only due to its orbital angular momentum L . On the other hand, it is also easy to see that a longitudinal X_μ is not produced. If the semi-annihilation had been s -wave, it would be subject to strong constraints from CMB data [31] and Fermi-LAT measurements of gamma ray emission coming from the galactic center, halos, or dwarf galaxies [32]: our model for semi-annihilation is free from such constraints.

3.2 Annihilation Channel

In addition to the semi-annihilation process — which plays a central role in determining the dark pion abundance and arises from the topological interaction in Eq. (2.4) — there are other relevant processes induced by additional operators in the chiral Lagrangian. In particular, it has been assumed in the literature that dark matter remains in kinetic equilibrium with the Standard Model during freeze-out via self-annihilation processes [17]. In our model, kinetic equilibrium can be maintained through scattering processes such as $X\chi \rightarrow X\chi$. The crossed diagram also contributes to the annihilation process $\chi\chi \rightarrow XX$, which may compete with the semi-annihilation channel. It is therefore essential to study the $\chi\chi XX$ coupling in general.

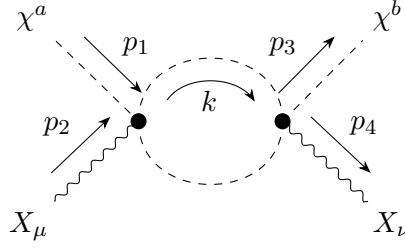


Figure 1: One-loop contribution to elastic channel $\chi^a \chi^a \leftrightarrow X X$, mediated through two insertions of the topological interaction.

3.2.1 NDA Estimate

Using naïve dimensional analysis, we estimate the size of the operators responsible for the $\chi\chi XX$ interaction as follows

$$\mathcal{L}_{\chi\text{PT}} \supset \left(\frac{e_B}{16\pi^2 f_\chi} \right)^2 \left(\lambda_1 \left(\partial_\alpha U^\dagger \right) (\partial^\alpha U) X_{\mu\nu} X^{\mu\nu} + \lambda_2 \left(\partial_\alpha U^\dagger \right) (\partial^\nu U) X_{\mu\nu} X^{\mu\alpha} \right), \quad (3.5)$$

with $\lambda_{1,2} \sim O(1)$. We next present estimates of these loop-induced couplings from both the IR and UV sides, and show they agree with this NDA expectation. We then discuss their consequences regarding the annihilation and thermalisation processes.

3.2.2 IR Estimate

We here estimate the loop-induced contribution within the low-energy EFT to the elastic channel $\chi^a X_\mu \leftrightarrow \chi^b X_\nu$. Inserting twice the topological operator as shown in Fig. 1, using the $\mathfrak{su}(N_f)$ Lie algebra identity $f_{acd}f_{cdb} = -N_f \delta_{ab}$ to sum over the flavour indices of the dark pions in the loop, and doing an integral over the loop momenta, we find the following one-loop amplitude

$$i\mathcal{M}_{\chi^a X \rightarrow \chi^b X} = \left(\frac{e_B}{2\pi^2 f_\chi^3} \right)^2 N_f \delta_{ab} \epsilon^{\mu\lambda\rho\sigma} \epsilon^{\nu\alpha\beta\gamma} p_{1\sigma} p_{2\mu} \varepsilon_{2\lambda}(p_2) p_{3\gamma} p_{4\nu} \varepsilon_{4\alpha}(p_4) \\ \times \int \frac{d^4 k}{(2\pi)^4} \frac{k_\rho k_\beta}{(m_\chi^2 - k^2)(m_\chi^2 - (k - p_1 - p_2)^2)}, \quad (3.6)$$

where k is the loop momentum, and $p_{1,3}$ ($p_{2,4}$) are the dark pion (photon) momenta. By Lorentz invariance, the loop integral can be decomposed into two pieces

$$\int \frac{d^4 k}{(2\pi)^4} \frac{k_\rho k_\beta}{(m_\chi^2 - k^2)(m_\chi^2 - (k - p_1 - p_2)^2)} \equiv \frac{1}{4} g_{\rho\beta} I + (p_1 + p_2)_\rho (p_3 + p_4)_\beta J. \quad (3.7)$$

The piece J will not contribute to the matrix element when contracted with the epsilon tensors, due to antisymmetry and the appearance of momenta in the matrix element written above. The important loop integral to keep is therefore the scalar integral

$$I(s, m_\chi) := \int \frac{d^4 k}{(2\pi)^4} \frac{k^2}{(m_\chi^2 - k^2)(m_\chi^2 - (k - p_1 - p_2)^2)}, \quad (3.8)$$

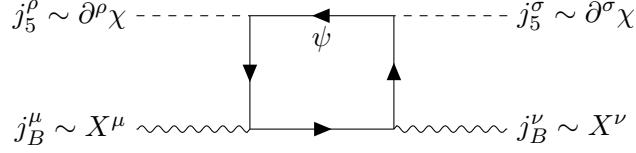


Figure 2: A one-loop diagram contribution to the 4-point function $\langle j_5^\rho j_5^\sigma j_B^\mu j_B^\nu \rangle$ as estimated from the UV – see main text. All permutations among the vertices need to be added.

which is a function of the dark pion mass m_χ and the kinematic Mandelstam $s = (p_1 + p_2)^2$.

The loop integral $I(s, m_\chi)$ has mass-dimension 2, reflecting a naïve quadratic divergence. We can obtain an order of magnitude estimate by cutting off the loop integral at $k = \Lambda \gg m_\chi, \sqrt{s}$ and keeping the leading part coming from the quadratic divergence, giving $I(s, m_\chi) \approx \Lambda^2/(4\pi)^2$. The coefficient becomes

$$\frac{N_f}{4} \left(\frac{e_B}{2\pi^2 f_\chi^3} \right)^2 \frac{\Lambda^2}{(4\pi)^2} \approx N_f \frac{e_B^2 \Lambda^2}{(4\pi f_\chi)^6} . \quad (3.9)$$

The cut-off dependence of this IR estimate suggests the $\chi\chi XX$ coupling comes from the strong dynamics.

3.2.3 UV Estimate

Here we attempt to estimate the $\chi\chi XX$ coupling from the UV theory. The interpolating field for the pion is the axial current $f_\chi \partial^\mu \chi^a \approx j_5^{a\mu} = \bar{Q} \gamma^\mu \gamma_5 T^a Q$, and the $\chi\chi XX$ interaction comes from the box diagram of the quark loop $\langle j_5^\mu j_5^\nu j_B^\rho j_B^\sigma \rangle$ shown in Fig. 2. Because of the gauge invariance, two powers of external momenta are extracted out of the integral, and it is quadratically IR divergent. Cutting it off at Λ as the “matching scale” between the UV theory and the chiral Lagrangian, the coefficient is

$$\frac{e_B^2}{N_c} \frac{1}{(4\pi)^2} \frac{1}{\Lambda^2} \frac{1}{f_\chi^2} = \frac{1}{N_c} \frac{e_B^2}{(4\pi f_\chi)^2 \Lambda^2} . \quad (3.10)$$

Apart from model-dependent factors of N_f, N_c , Eqs. (3.9) and (3.10) become the same if the theories are matched at $\Lambda = 4\pi f_\chi$, namely where the theory is strongly coupled. We consider this to be a good estimate.

3.2.4 Annihilation Cross-Section

We are now able to estimate the contribution of the annihilation channel to the evolution of the dark pion abundance using the effective operators in Eq. (3.5), parametrising the unknown aspects of the strong dynamics through the corresponding Wilson coefficients λ_1 and λ_2 , which we assume to be of order unity.

As in the case of semi-annihilation, we defer the computational details to App. B, and provide here the expression for the $\chi\chi \rightarrow XX$ cross-section and its corresponding thermal

average. In the limit of the dark photon being massless, we find

$$\sigma_{\chi\chi\rightarrow XX} = \frac{1}{N_f^2 - 1} \left(\frac{e_B}{16\pi^2 f_\chi^2} \right)^4 \frac{1}{4\pi} s \sqrt{\frac{s}{s - 4m_\chi^2}} \times \left[(s - 2m_\chi^2)^2 (\text{Re}(\lambda_1 \lambda_2^*) + 2|\lambda_1|^2) - \frac{1}{120}(92m_\chi^4 - 76m_\chi^2 s + 17s^2)|\lambda_2|^2 \right]. \quad (3.11)$$

The full expression for the thermally averaged cross-section (still in the massless dark photon limit) is then given in Eq. (B.6); as before, it is most instructive to expand this result in powers of $x = m_\chi/T$, to obtain

$$\langle\sigma v\rangle_{\chi\chi\rightarrow XX} \approx \frac{1}{N_f^2 - 1} \left(\frac{e_B}{16\pi^2 f_\chi^2} \right)^4 \frac{m_\chi^6}{\pi} |4\lambda_1 + \lambda_2|^2 \left(1 + \frac{15}{8}x^{-1} + \mathcal{O}(x^{-2}) \right). \quad (3.12)$$

We observe that the annihilation process now contains a velocity-independent leading order piece, unlike what we found for semi-annihilation, meaning it is in principle subject to constraints coming from indirect detection and CMB data. However, in contrast to the tree-induced semi-annihilation process, the annihilation channels in this model are loop-suppressed and become relevant only in the regime where $m_\chi > 4\pi f_\chi$. We can assess this numerically. For instance, considering the CMB constraints, the annihilation cross section satisfies $\langle\sigma v\rangle_{\chi\chi\rightarrow XX} \lesssim 3 \times 10^{-26} \text{ cm}^3/\text{s}$, for $m_\chi > 1 \text{ GeV}$ and $e_B < 10^{-2}$, which remains below the sensitivity of the Planck satellite even when $m_\chi = 4\pi f_\chi$ [43].

Generally, the relative importance of annihilations compared to semi-annihilations can be quantified via the ratio

$$\frac{\langle\sigma v\rangle_{\chi\chi\rightarrow XX}}{\langle\sigma v\rangle_{\chi\chi\rightarrow \chi X}} \simeq \frac{|4\lambda_1 + \lambda_2|^2 e_B^2}{64\pi^4 N_f} \frac{m_\chi^2}{f_\chi^2} x, \quad (3.13)$$

from which we see that annihilations can become comparable to semi-annihilations in determining the relic abundance when $m_\chi > 4\pi f_\chi$ assuming benchmark values $\lambda_{1,2} \sim \mathcal{O}(1)$, $e_B \sim 0.1$, and $x = x_f \sim \mathcal{O}(20)$ at freeze-out. Consequently, in the parameter space where dark pions can constitute viable dark matter candidates — namely $m_\chi < 4\pi f_\chi$, as discussed in the following section — the annihilation channel is expected to provide only a subdominant contribution. This expectation is explicitly confirmed in the numerical analysis of §4.2.

3.3 Kinetic Equilibrium

The elastic scattering process $X\chi \rightarrow X\chi$ thermalises the dark pions with the Standard Model bath since the dark photon X_μ kinetically mixes with the ordinary photon. Throughout this paper, we assume that X_μ maintains thermal equilibrium with the Standard Model. It requires only a modest lower limit on the kinetic mixing

$$\epsilon \gtrsim \alpha^{-1} \left(\frac{T}{M_{\text{Pl}}} \right)^{1/2} \simeq 4 \times 10^{-8} \left(\frac{T}{\text{GeV}} \right)^{1/2}, \quad (3.14)$$

where α is the electromagnetic fine-structure constant.

To identify the region of the (m_χ, f_χ) parameter space where dark pion thermalisation is effective, we compare the interaction rate of the $X\chi \rightarrow X\chi$ process with the Hubble expansion rate. The thermalisation condition requires

$$\Gamma_{X\chi \rightarrow X\chi} = n_\chi \langle \sigma v \rangle_{X\chi \rightarrow X\chi} \gtrsim H, \quad (3.15)$$

where n_χ is the dark pion number density and H is the Hubble parameter.

The cross-section can be obtained using the matrix elements in Eqs. (B.2) and (B.3) and the convolution with the final state phase-space. In the limit of the massless dark photon X_μ , we find

$$\begin{aligned} \sigma_{X\chi \rightarrow X\chi} &= \frac{1}{64\pi s} \left(\frac{e_B}{16\pi^2 f_\chi^2} \right)^4 \left(1 - \frac{m_\chi^2}{s} \right)^4 \\ &\times \left[|4\lambda_1 + \lambda_2|^2 \left(\frac{1}{5} (s - m_\chi^2)^4 - (s - m_\chi^2)^2 s m_\chi^2 + \frac{4}{3} s^2 m_\chi^4 \right) + \frac{4}{3} |\lambda_2|^2 s^4 \right]. \end{aligned} \quad (3.16)$$

We are interested in whether the kinetic equilibrium between the dark pions and the SM bath is kept long enough until the onset of the dark pion freeze-out, which occurs at temperatures $T \sim m_\chi/x_f$ with $x_f \sim \mathcal{O}(10 - 30)$ depending on the values of the parameters (with larger x_f achieved for larger dark pion masses). At these temperatures, we consider the dark pions to be non-relativistic, such that their relative velocity with dark photons is $v \sim 1$, and the center-of-mass energy can be approximated by

$$s = (p_\chi + p_X)^2 = m_\chi^2 + 2E_\chi E_X (1 - \cos \theta) \stackrel{\int d\theta}{\simeq} m_\chi^2 + 2m_\chi T, \quad (3.17)$$

where we used that $E_X \sim T$, $E_\chi \sim m_\chi + 3T/2$, and we integrated over the angle θ between the χ and X momenta assuming the uniform distribution.

Substituting this into Eq. (3.15) and using the assumed equilibrium distribution for the dark pions, their successful thermalisation at $T \sim m_\chi/x$ requires

$$\frac{(|4\lambda_1 + \lambda_2|^2 + |\lambda_2|^2) e_B^4}{12288 \sqrt{2} \pi^{21/2} x^{11/2}} e^{-x} \frac{m_\chi^9}{f_\chi^8} \gtrsim \frac{m_\chi^2}{x^2 M_{\text{Pl}}^2}. \quad (3.18)$$

The region of the (m_χ, f_χ) parameter space where kinetic equilibrium is not maintained through the elastic scattering channel is indicated by various shades of purple in Fig. 4. Each shade corresponds to the parameter space for which kinetic equilibrium persists only up to a given stage in the cosmological evolution, quantified by $x_f = m_\chi/T_{\text{FO}}$, with T_{FO} denoting the freeze-out temperature. The figure illustrates that, in general, elastic scattering via $\chi X \rightarrow \chi X$ is insufficient to sustain kinetic equilibrium between χ and the SM bath right up to the freeze-out moment. As a result, the DM temperature need not track that of the SM bath, potentially leading to a non-trivial thermal history for the dark sector [44] that we should account for, which we do in the following Subsection.

3.4 Self-Heating

Ref. [44] studied the consequences of DM going out of thermal equilibrium before freeze-out via semi-annihilation is completed, which will happen if the elastic $\chi X \rightarrow \chi X$ scattering is not efficient enough. They showed that, if the semi-annihilation is s -wave, the $\chi\chi \rightarrow X\chi$ process starts to inject significant energy into the final state χ -particle as χ becomes non-relativistic, specifically $E_{\chi,f} = m_\chi \left(\frac{5}{4} - \frac{m_\chi^2}{4m_X^2} \right) \equiv \gamma m_\chi$, leading to an increase in the DM temperature *viz.* $T_\chi/T_{\text{SM}} \approx \frac{2}{3}(\gamma - 1)x_f$ that can be as large as a factor 5 to 6 enhancement.

However, the authors of Ref. [45] concluded that there is no significant self-heating when the semi-annihilation is in the p -wave, which is the case for our model. This is because the kinetic energy density of dark matter χ redshifts adiabatically as

$$\rho_K = \left\langle \frac{p^2}{2m_\chi} \right\rangle n_\chi \propto a^{-5}, \quad (3.19)$$

while the injection due to the semi-annihilation is

$$\Delta\rho_K \approx \frac{1}{H} \langle \sigma v \rangle n_\chi^2 \propto a^2 a^{-2L} a^{-6} \quad (3.20)$$

which is important for $L = 0$ (s -wave) at later times but not for $L \geq 1$ (p -wave and beyond). At the same time, the final abundance of dark matter is not modified more than 10% by going out of equilibrium (in either the s -wave or p -wave case).

Therefore, we will not discuss the possibility of self-heating any further in our paper, and we are reassured that even in parameter space regions for which thermalisation is not maintained we do not expect a large correction to the DM relic abundance.

4 Boltzmann Equation

In this section, we solve the Boltzmann equation governing the evolution of the dark pion number density n_χ , taking into account the processes considered in the previous Section, and demonstrate that dark pions can account for the observed dark matter abundance. We identify the combinations of model parameters that yield the correct relic density and delineate the viable region of parameter space. This region is bounded by several theoretical and observational constraints: the validity of the EFT, limits on N_{eff} , bounds from dark pion self-interactions, and the requirement that kinetic equilibrium with the Standard Model is maintained long enough to ensure the robustness of our predictions.

In the presence of dark pion annihilations ($\chi\chi \rightarrow XX$) and semi-annihilations ($\chi\chi \rightarrow \chi X$), the Boltzmann equation for the dark pion number density n_χ reads

$$\frac{dn_\chi}{dt} + 3Hn_\chi = -\langle \sigma v \rangle_{\chi\chi \rightarrow XX} (n_\chi^2 - n_\chi^{\text{eq}2}) - \langle \sigma v \rangle_{\chi\chi \rightarrow \chi X} (n_\chi^2 - n_\chi n_\chi^{\text{eq}}), \quad (4.1)$$

where H is the Hubble parameter and n_χ^{eq} is the equilibrium number density distribution. For convenience, it is more suitable to rewrite Eq. (4.1) as

$$\frac{dY_\chi}{dx} = -\sqrt{\frac{\pi g_*}{45}} \frac{M_{\text{Pl}} m_\chi}{x^2} [\langle \sigma v \rangle_{\chi\chi \rightarrow XX} (Y_\chi^2 - Y_\chi^{\text{eq}2}) + \langle \sigma v \rangle_{\chi\chi \rightarrow \chi X} (Y_\chi^2 - Y_\chi Y_\chi^{\text{eq}})], \quad (4.2)$$

where we defined a comoving number density, or yield, $Y_\chi = n_\chi/s$, with s being the entropy density of the relativistic degrees of freedom, and the evolution parameter is $x = m_\chi/T$. Here M_{Pl} is the Planck mass, g_* is the effective number of relativistic degrees of freedom, and the equilibrium yield Y_χ^{eq} is a function of the evolution parameter x , given by

$$Y_\chi^{\text{eq}} = \frac{45}{4\pi^4 g_*} x^2 K_2(x), \quad (4.3)$$

with $K_2(x)$ being the modified Bessel function of the second order.

We solve Eq. (4.2) numerically by substituting the explicit expressions for the thermally averaged cross-sections $\langle\sigma v\rangle_{\chi\chi\rightarrow\chi X}$ and $\langle\sigma v\rangle_{\chi\chi\rightarrow XX}$ in Eqs. (A.11) and (B.6), respectively. We find that there is indeed a viable parameter space that allows us to set the correct relic abundance for dark pions

$$\Omega_\chi h^2 \approx \frac{2 m_\chi Y_\infty}{3.6 \cdot 10^{-9} \text{ GeV}} \approx 0.12, \quad (4.4)$$

with Y_∞ defined as a solution of Eq. (4.2) in the limit $x \rightarrow \infty$.

We show the evolution of Y_χ for two benchmark values of the model parameters in Fig. 3, namely:

$$\text{Benchmark 1: } m_\chi = 1 \text{ GeV}, \quad f_\chi = 2.8 \text{ GeV}, \quad (4.5)$$

$$\text{Benchmark 2: } m_\chi = 100 \text{ GeV}, \quad f_\chi = 27.2 \text{ GeV}, \quad (4.6)$$

and taking $e_B = N_f/2 = \lambda_1 = \lambda_2 = 1$ for both benchmarks. The solid red line represents the numerical solution of the Boltzmann equation using the full x -dependence of the thermally averaged cross sections. In contrast, the solid orange line corresponds to the solution obtained by retaining only the leading-order term in the velocity expansion of Eqs. (3.4) and (3.12). The resulting difference in the final relic abundance is at the level of 10% - 15%, consistent with the expectation that dark pions are nearly non-relativistic at freeze-out.

In the following Subsections we compare the contributions of semi-annihilation and annihilation processes in determining the final dark pion abundance. We show that, within the relevant region of parameter space, annihilation processes are subdominant and can be safely neglected. This simplification enables us to obtain a more transparent analytical understanding of the parameter dependencies, and clarifies the conditions under which dark pions constitute a viable dark matter candidate.

4.1 Semi-Annihilation Contribution

Let us start by analysing the Boltzmann equation keeping only the contribution from the semi-annihilation process, *i.e.* by setting $\langle\sigma v\rangle_{\chi\chi\rightarrow XX} = 0$ in the Boltzmann equation (4.2). To better understand how various parameters affect the final abundance, we can use the semi-analytic solution for $\Omega_\chi h^2$ derived in [17]. For the case of semi-annihilations, the freeze-out value x_f can be found by solving the equation

$$x_f = \log \left[0.038c(c+1) \frac{m_\chi M_{\text{Pl}}}{\sqrt{g_*} x_f} \langle\sigma v\rangle_{\chi\chi\rightarrow\chi X} \right], \quad (4.7)$$

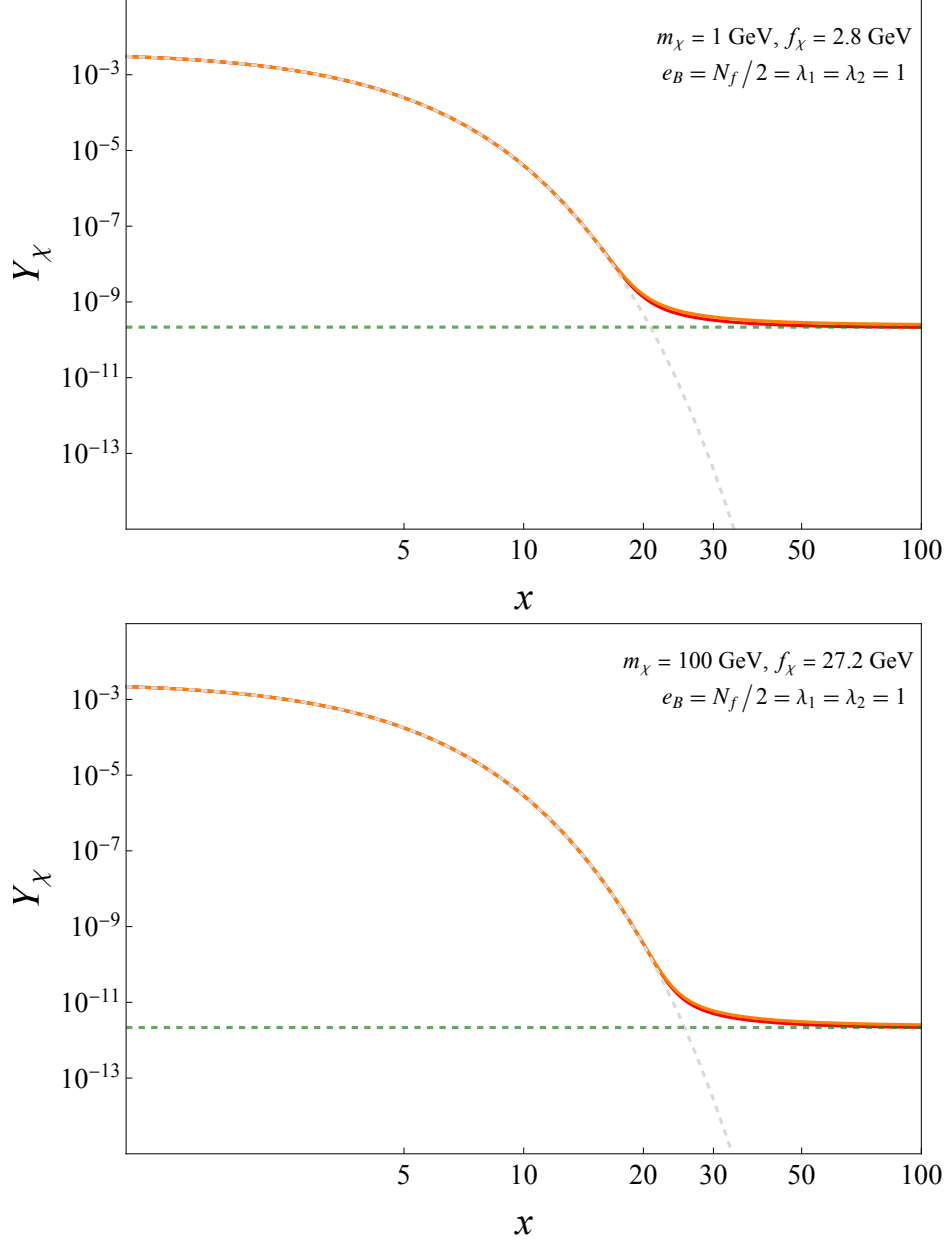


Figure 3: The dark pion yield Y_χ as a function of $x = m_\chi/T$ for two benchmark parameter sets. The solid red (orange) line represents the numerical solution of the Boltzmann equation (4.2) using the full (leading-order) x -dependence of the thermally averaged cross sections. The observed relic abundance is achieved for the Y_χ value denoted by the dashed green line, while the grey dashed line shows the equilibrium distribution $Y_\chi^{\text{eq}}(x)$.

where $c \in \mathbb{R}$ is a constant that encodes the information on the offset of the freeze-out; it is defined numerically through

$$Y_\chi(x_f) - Y_\chi^{\text{eq}}(x_f) = c Y_\chi^{\text{eq}}(x_f). \quad (4.8)$$

The value of x_f exhibits only a logarithmic dependence on $\langle\sigma v\rangle_{\chi\chi\rightarrow\chi X}$, and, for values of the model parameters yielding the correct relic abundance, it typically lies in the range $x_f \in [15, 30]$. Its precise value can be determined numerically and subsequently used to compute the present-day dark pion energy density

$$\Omega_\chi h^2 = 2 \times \frac{1.07 \times 10^{-9} \text{GeV}}{\sqrt{g_*} M_{\text{Pl}} J(x_f)}, \quad (4.9)$$

where

$$J(x_f) = \int_{x_f}^{\infty} \frac{\langle\sigma v\rangle_{\chi\chi\rightarrow\chi X}}{x^2} dx. \quad (4.10)$$

Using the form of $\langle\sigma v\rangle_{\chi\chi\rightarrow\chi X}$ in Eq. (3.4), the relic abundance in the case of semi-annihilations scales as

$$\Omega_\chi h^2 \propto \frac{N_f^2 - 1}{e_B^2 N_f} \frac{x_f^2}{\sqrt{g_*}} \frac{f_\chi^6}{m_\chi^4} \text{GeV}^{-2}. \quad (4.11)$$

Note that x_f itself depends on the model parameters, as can be seen in Eq. (4.7). Nevertheless, Eq.(4.11) provides a good analytical understanding of how the parameters need to be adjusted to yield the observed relic abundance. In particular, the contours in the (m_χ, f_χ) parameter space satisfying $\Omega_\chi h^2 = 0.12$ follow the scaling relation $f_\chi \propto e_B^{1/3} m_\chi^{2/3}$, as illustrated in Fig. 4 by the three solid lines corresponding to $e_B = \{0.1, 0.1^3, 0.1^5\}$.

4.2 Full Contribution

When both semi-annihilation and annihilation processes are included, the freeze-out moment x_f can be found by numerically solving the following equation [17]

$$x_f = \log \left[0.038c(c+1) \langle\sigma v\rangle_{\chi\chi\rightarrow\chi X} \frac{m_\chi M_{\text{Pl}}}{\sqrt{g_*} x_f} \right] + \log \left[1 + \frac{(c+2) \langle\sigma v\rangle_{\chi\chi\rightarrow XX}}{(c+1) \langle\sigma v\rangle_{\chi\chi\rightarrow\chi X}} \right]. \quad (4.12)$$

We present an analytic solution for x_f in the non-relativistic limit in App. C, retaining only the leading-order term in x^{-1} from each cross-section. Moreover, a comparison with numerical results for various benchmarks shows good agreement.

The impact of dark pion annihilations on the freeze-out value x_f appears as a subleading correction in the second term of Eq. (4.12), on top of the value set by the semi-annihilation process in Eq. (4.7). This is due to the one-loop suppression of $\langle\sigma v\rangle_{\chi\chi\rightarrow XX}$ relative to $\langle\sigma v\rangle_{\chi\chi\rightarrow\chi X}$. Therefore, as discussed in §3.2, annihilations significantly affect the value of x_f only when $m_\chi > 4\pi f_\chi$ and the two thermally-averaged cross-sections become comparable.

The same conclusion pertains for the present-day dark pion energy density. Indeed, Eq. (4.9) can be generalised to the case where both processes are kept track of [17]:

$$\Omega_\chi h^2 = 2 \times \frac{1.07 \times 10^{-9} \text{GeV}}{\sqrt{g_*} M_{\text{Pl}}} \left[\int_{x_f}^{\infty} \frac{\langle\sigma v\rangle_{\chi\chi\rightarrow\chi X} + \langle\sigma v\rangle_{\chi\chi\rightarrow XX}}{x^2} dx \right]^{-1}, \quad (4.13)$$

where again the annihilation contribution becomes relevant only when $\langle\sigma v\rangle_{\chi\chi\rightarrow XX} \approx \langle\sigma v\rangle_{\chi\chi\rightarrow\chi X}$, *i.e.*, when $m_\chi > 4\pi f_\chi$.

As it turns out, numerical solutions of the Boltzmann equation, including both semi-annihilation and annihilation contributions, consistently yield values of m_χ that reproduce the observed relic abundance while satisfying $m_\chi < 4\pi f_\chi$. This naturally places us in a regime where semi-annihilations dominate, which explains why the approximation in Eq. (4.11), derived under the assumption of semi-annihilations only, accurately describes the solid contours in Fig. 4.

4.3 Parameter Space

We are now ready to put things together, summarising all the important constraints in Fig. 4. Since semi-annihilations mainly determine the dark pion relic abundance, the key parameters are m_χ , f_χ , e_B , and the dark photon mass m_X . We find that the interesting dark pion mass range, capable of yielding $\Omega_\chi h^2 = 0.1200 \pm 0.0024$ [43], is

$$m_\chi \in [10^{-3}, 10^3] \text{ GeV}, \quad \text{for } e_B = 0.1, \quad (4.14)$$

as indicated by the solid dark green contour in Fig. 4. Reducing e_B lowers the required values of f_χ to achieve the correct relic abundance, which in turn shifts the interesting m_χ mass range downward – as shown by the lighter green solid contours. These contours, for $e_B = 0.1^3$ and smaller, begin to enter the region where $m_\chi > 4\pi f_\chi$, marked by the gray shaded area in Fig. 4, and thus fall outside the EFT range of validity (also the area where annihilations would dominate).

Dark Photon Mass Effects

So far we have restricted to the case in which the dark photon is massless. The effect of introducing a non-zero dark photon mass m_X becomes significant only when it approaches the dark pion mass. Of course, the semi-annihilation channel $\chi\chi \rightarrow \chi X$ channel closes in the limit $m_X \rightarrow m_\chi$, as can be checked from Eq. (A.8) in the Appendix, and so we expect that turning on a non-zero m_X for fixed m_χ requires a larger coupling, *i.e.* a reduced value of f_χ , to fit the same relic abundance. Specifically, the required value of f_χ follows the approximate scaling relation $f_\chi \propto f_\chi^{(0)} \Delta^{1/4}$, where $f_\chi^{(0)}$ is the value in the massless dark photon limit and $\Delta = (m_\chi - m_X)/m_\chi$ is the mass-splitting. Nevertheless, as long as $\Delta > 0.2$, the effect of a nonzero m_X on the final dark pion yield remains below 20%. Therefore, we adopt the natural assumption of non-degeneracy between the dark pion and photon and set $m_X = 0$ throughout.

Constraint from BBN

Another consideration is the limit that $\Delta N_{eff} \lesssim 0.4$ at the time of Big-Bang Nucleosynthesis (BBN) [46], which leads to a constraint on m_X (and so indirectly on m_χ too) as follows. If the dark photon is lighter than an MeV and stays in thermal equilibrium at the time of BBN, it would contribute $\Delta N_{eff} = \frac{8}{7}$, not allowed by the current limit. We therefore have to assume that the dark photon decays away before the temperature comes down to $T \simeq 2$ MeV,

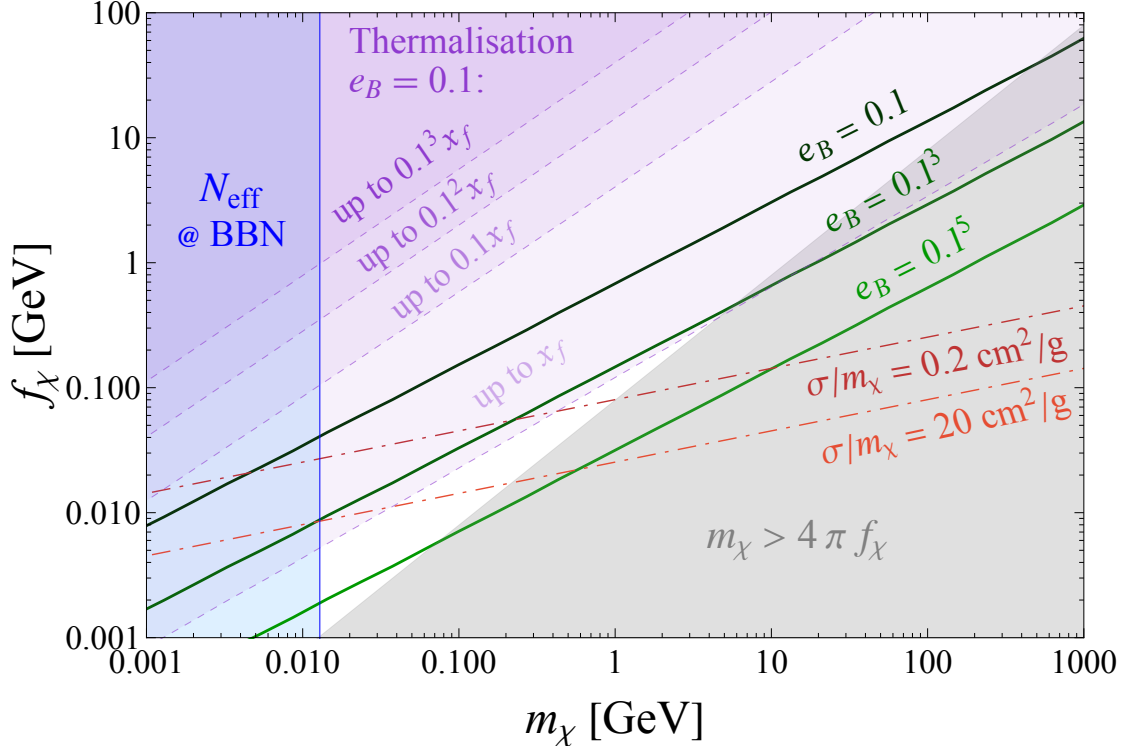


Figure 4: Solid lines in the (m_χ, f_χ) plane indicate the values for which the correct relic abundance of dark pions is achieved: black for $e_B = 0.1$, dark green for $e_B = 0.1^3$, and green for $e_B = 0.1^5$ ($N_f = 2$ always). The gray shaded region corresponds to the regime where $m_\chi > 4\pi f_\chi$. The blue region indicates the constraint from N_{eff} at the time of BBN, excluding values $m_\chi \lesssim 10$ MeV. Purple regions mark areas of parameter space where thermalisation of dark pions fails to occur by a given point in the cosmic evolution. Different dashed lines represent the boundaries beyond which successful thermalisation is achieved only up to the shown temperatures, expressed in units of $x_f = m_\chi/T_{\text{FO}}$, with T_{FO} being the freeze-out temperature. Note, however, that the lack of thermalisation is not a problem because there is no self-heating thanks to the p -wave nature of semi-annihilation. Finally, the dash-dotted red lines indicate the constraints from the self-interactions among dark pions.

requiring its mass to be above several MeV. Since the dark pion is supposed to be heavier than the dark photon, we conservatively require $m_\chi \gtrsim 10$ MeV, shown as the blue excluded region in Fig. 4.

Dark Matter Self-Interactions

As already mentioned at the end of the previous Section, lowering the gauge coupling e_B requires a lower f_χ for fixed m_χ in order to keep $\Omega_\chi h^2 \approx 0.12$. However, for $N_f = 2$ flavours of dark quark, the chiral Lagrangian predicts self-interactions among the dark pions that become too large for low f_χ values. To quantify this effect, we report the partial-wave amplitudes $a_{L=0, I=0} = \frac{7m_\chi}{16\pi f_\chi^2}$ and $a_{L=0, I=2} = -\frac{m_\chi}{8\pi f_\chi^2}$ for $\chi\chi \rightarrow \chi\chi$ scattering in the isospin channels $I = 0, 2$. The isospin channel $I = 1$ has only a p -wave scattering, which can be

neglected for our purpose. Among the three dark pions, the flavour-averaged self-interaction cross section is

$$\sigma_{\chi\chi\rightarrow\chi\chi}^{\text{flavour-avg.}} = \frac{1}{9}4\pi a_{L=0,I=2}^2 + \frac{5}{9}4\pi a_{L=0,I=2}^2 = \frac{23m_\chi^2}{192\pi f_\chi^4}. \quad (4.15)$$

Contours of constant $\sigma_{\chi\chi\rightarrow\chi\chi}^{\text{flavour-avg.}}$ are shown by dash-dotted red lines in Fig. 4. Note, however, that the dark pions may scatter resonantly with a strong velocity dependence [47] through a ρ -like [48] or σ -like [49] state, and hence typical upper limits such as $\sigma/m_\chi < 0.2 \text{ cm}^2/\text{g}$ (see, *e.g.*, [50] for a recent analysis) may not apply.

5 Phenomenology

Having delineated the viable region of parameter space that fits the DM relic abundance, and taking into account other cosmological constraints, we now turn to discuss how this model of DM semi-annihilation via topological freeze-out can be searched for experimentally.

5.1 Direct and Indirect Detection

Firstly, and as we have already alluded to, the indirect detection of our dark pion DM via their annihilation $\chi\chi \rightarrow XX \rightarrow \gamma\gamma$ at the galactic center, halos, or dwarf galaxies, is suppressed by the p -wave nature of the scattering. The constraints are therefore negligible even for the sub-GeV DM mass range. Direct detection is also highly suppressed because the process involves many loops. This is a key feature of our model, and traces back to the topological nature of the $\chi\chi\chi X$ vertex (which lends it a three-derivative suppression).

On the other hand the X_μ gauge boson, which is kinetically mixed with the photon, can be produced at accelerators and hence allows for interesting phenomenology. We turn our attention to accelerator-based searches below.

5.2 Dark Photon Bounds

Recall the bound (3.14) derived above for the dark photon to remain in equilibrium with the SM through the vector portal. Evaluating this at the DM freeze-out temperature gives the following ball-park lower bound on the kinetic mixing parameter ϵ ,

$$\epsilon \gtrsim 10^{-9} \frac{m_\chi}{\text{GeV}}. \quad (5.1)$$

For m_χ light enough, we can evade bounds from astrophysics to allow for this kinetic mixing to be large enough: roughly, we need to go down to $m_\chi \lesssim 10^{-14} \text{ eV}$. But, as we have seen, for such light dark photon masses we would contravene the bounds from BBN, and so we focus our interest on the allowed region with heavier dark photon mass, $m_\chi \gtrsim 1 \text{ GeV}$. Here the experimental bound on the kinetic mixing parameter is very weak compared to (5.1), and comes from various collider measurements – beam-dump experiments, BaBar, Belle, LEP, and the LHC experiments – the most relevant of which are discussed below. We refer the reader to Refs. [48, 51] for compilations of experimental limits.

5.3 Collider Phenomenology

In our model, dark sector states can be produced at collider experiments principally through the kinetic mixing portal – although there is also the possibility of a Higgs portal that mixes the $U(1)_B$ -breaking scalar ϕ with the SM Higgs boson *viz.* $\mathcal{L} \supset \kappa |H|^2 |\phi|^2$.

The production of DS particles via the vector portal is suppressed by ϵ^2 , while in the case of a Higgs portal the production rates are governed by the Higgs mixing parameter κ . Here, we mostly focus on the case where the vector portal is the dominant one. Depending on the values of ϵ and e_B the dark photon can either decay to two dark quarks ($\Gamma_{X \rightarrow Q\bar{Q}} \propto e_B^2$) or two leptons ($\Gamma_{X \rightarrow \ell\bar{\ell}} \propto \epsilon^2$). As we are interested in the case $m_X < m_\chi$ and χ are the lightest particles of the confining sector, two dark quarks are always produced via an off-shell dark photon. Once produced, they will undergo dark sector shower and hadronisation, leading to dark pions in the final state.

The collider signatures of the model depend on the hierarchy of e_B and ϵ as well as the lifetime of X_μ . Possible signatures include mono-photon (via the Feynman diagrams shown in Fig. 5), mono-jet, exotic Higgs decays $h \rightarrow (\gamma+) inv.$ and four lepton final states, or a dark shower from the decay to dark quarks.

Mono-photon

For dark photon masses towards the higher end of our preferred mass range, there are important searches with mono-photon final states at the LHC *e.g.* in [52], where bounds are presented for two different benchmark choices of mediator-lepton, mediator-quark and mediator-dark matter couplings, $\{g_l, g_q, g_\chi\}$. For our model, these bounds can be cast into the $\{m_\chi, m_X\}$ plane, excluding the mass range $\{m_\chi, m_X\} \in \{[80, 425], [0, 840]\}$ GeV for couplings $\{0, 0.25, 1\}$, and excluding $\{m_\chi, m_X\} \in \{[15, 175], [0, 350]\}$ GeV for couplings $\{0.01, 0.1, 1\}$. But note that we cannot directly use these benchmarks because, in our case, both the dark photon coupling to leptons and quarks are proportional to ϵ^2 and cannot be taken independently. Instead, we make use of the limits on the fiducial cross section $\sigma \times \epsilon_{\text{eff}} \times A \lesssim 0.53 - 2.45$ fb depending on the signal region, with A the acceptance and ϵ_{eff} the efficiency. Assuming the mono-photon final state occurs from photon pair production, where one of the photons mixes to a dark photon, this sets a limit of $\epsilon \lesssim 5 \times 10^{-3} - 10^{-2}$. The mono-photon final state also arises from s-channel dark photon production via kinetic mixing and an initial-state radiation photon. This process is proportional to $\epsilon^2 \times e_B$ and additionally suppressed due to the dark photon being produced off-shell. A search for a heavy scalar resonance, *e.g.* the $U(1)$ breaking scalar, in the mono-photon final state can be found in [53]. Expected sensitivities for the mono-photon final states at high-luminosity LHC (HL-LHC) are discussed in [54], while prospects of this signature at a future muon collider are considered in [55].

Mono-photon searches have also been performed at B factories, which provide the best constraints for lighter mass dark particles. A search at BaBar excludes $\epsilon \leq 10^{-3}$ for 10^{-3} GeV $< m_X < 2$ GeV. The bound extends up to $m_X \leq 8$ GeV limiting ϵ between a few times 10^{-4}

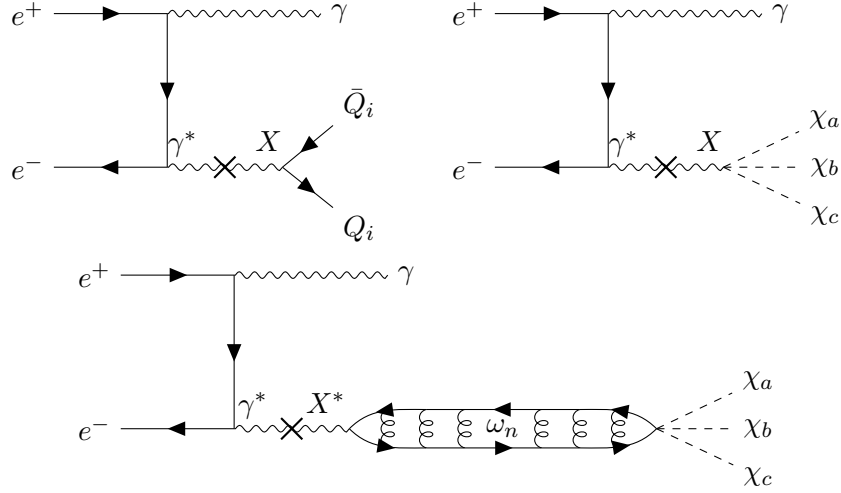


Figure 5: Mono-photon production in e^+e^- collisions. The cross representations the kinetic mixing vertex $\gamma^* \rightarrow X$, which carries a suppression by the parameter ϵ . In the régime $s \gg f_\chi$, where \sqrt{s} is the relevant centre-of-mass energy of the collider (~ 91 GeV at a Z factory, or ~ 11 GeV at a B factory), the dark photon b decays to a pair of dark quarks. At lower (relative) energy, $s < f_\chi$ or so, the dark photon can decay to a trio of pions via the $\chi\chi\chi X$ semi-annihilation vertex that sets the DM relic abundance in this theory; alternatively, the off-shell dark photon may mix into a spin-1 resonance ω_n of the dark sector, enabling a ‘dark spectroscopy’ search strategy.

and 10^{-3} [56]. It is expected that Belle II will improve this bound by nearly an order of magnitude to reach $\epsilon \lesssim 3 \times 10^{-4}$ [57].

Dark Spectroscopy

In addition, at e^+e^- colliders such as Belle and BaBar, or indeed at a future high-energy lepton collider such as FCC-ee, kinematic constraints provide more information to pin down invisible decays. Consider $e^+e^- \rightarrow \gamma X^*$, where the off-shell dark photon X^* mixes into ω -like resonances – see Fig. 5. Here the energy of the visible photon entirely determines the invariant mass of the invisible system:

$$M_{\text{inv}}^2 = s \left(1 - \frac{2E_\gamma}{\sqrt{s}} \right). \quad (5.2)$$

Therefore, the energy distribution of the mono-photon signal events would exhibit a set of resonant peaks due to ω -resonances in the DS, mirroring states such as $\omega(782)$, $\omega(1420)$, $\omega(1650)$, and $\omega(2220)$ in the case of visible QCD. In addition, the dark sector may well include additional heavier quarks, giving further peaks for resonances analogous to the J/ψ and so on. Observing such a spectrum of resonances would, in principle, determine the number of colours, flavours, and quark masses without observing any of the states directly – clearly a fascinating possibility that was proposed in [58, 59].

Exotic Higgs Decays

Higgs decays to visible and dark photons were searched for *e.g.* in [60, 61]. The current limit on this decay is $\text{Br}(h \rightarrow \gamma X) \lesssim 0.029$ [62]. Similarly, the bound on invisible Higgs decays is $h \rightarrow \text{inv.} < 10.7\%$ [62]. From $\text{Br}(h \rightarrow \gamma X) \sim \text{Br}(h \rightarrow \gamma\gamma) \times \epsilon^2$ and $\text{Br}(h \rightarrow XX) \sim \text{Br}(h \rightarrow \gamma\gamma) \times \epsilon^4$, one can infer bounds on the kinetic mixing parameter of order $\epsilon \lesssim \mathcal{O}(1)$ – rather weak.

At the HL-LHC, as well as future higgs factories such as FCC-ee and ILC the invisible higgs branching fraction can be probed to $\mathcal{O}(10^{-2} - 10^{-3})$ [63–65]. With $\text{Br}(h \rightarrow XX) \sim \text{Br}(h \rightarrow \gamma\gamma) \times \epsilon^4$ this improving the reach on ϵ in our model by about an order of magnitude.

Mono-jet

The mono-jet final state originates from s -channel dark photon production with an initial-state radiation jet. Both ATLAS and CMS have searched for the mono-jet final state [66, 67]. In [67], the search was interpreted for a vector mediator with couplings to quarks $g_q(\propto \epsilon) = 0.25$ and couplings to dark matter $g_\chi (= e_B) = 1$, excluding $m_\chi \lesssim 115$ GeV for massless dark photons up to $m_\chi \lesssim 300$ GeV for $m_X \sim 575$ GeV. These bounds will loosen for smaller values of ϵ . In addition, for $e_B = 1$ and $m_\chi = m_X/3$ limits on g_q are given ranging from 2×10^{-2} for $m_X = 100$ GeV to 0.3 for $m_X = 2$ TeV. For $m_X < 2m_\chi$ these limits weaken.

LHC mono-jet limits from LHC have been scaled for HL-LHC projecting $m_\chi \lesssim 200$ GeV exclusion for various dark matter-mediator coupling choices [68].

Leptonic Decays

If X_μ decays promptly and ϵ is not too small, we will see leptonic final states. A search for a low-mass resonance decaying to muons sets limits $\epsilon \lesssim 2 \times 10^{-3}$ for $m_X < 80$ GeV and $\epsilon \sim 3 \times 10^{-3} - 5 \times 10^{-3}$ for $m_X = 100 - 200$ GeV [69]. Similarly, a search for a low-mass resonance in Higgs decays to four leptons final state sets limits on $\text{Br}(H \rightarrow XX) \times \text{Br}(X \rightarrow ee \text{ or } \mu\mu)^2 \lesssim 2 \times 10^{-6}$ [70] leading to $\mathcal{O}(1)$ bounds on ϵ . Assuming a Higgs portal with $\kappa \gg \epsilon$, limits on $\kappa \lesssim 10^{-4} - 10^{-3}$ for $m_X \sim 5 - 60$ GeV were obtained.

Prospects of searches for leptonically decaying dark photons can be found for HL-LHC and future electron-positron colliders in [71, 72]. It is expected that these machines can probe $\epsilon \sim \mathcal{O}(10^{-2} - 10^{-3})$ via Drell-Yan production of dark photons. If $\text{Br}(h \rightarrow XX) \sim 0.5\%$ the leptonic decays will be able to probe $\epsilon \sim 10^{-9} - 10^{-6}$ at HL-LHC.

Semi-visible lepton jets

Finally, an interesting signature can arise when X_μ decays promptly to dark quarks, which shower and form dark hadrons, but also emit dark photons as part of the shower process. Thus, part of the shower can become visible when some of the dark photons decay back into SM leptons. The resulting signature consists of a collimated spray of (soft) leptons in association with a large amount of missing energy in the same direction, similar to a semi-visible jet [73, 74].

6 Conclusion and Outlook

In this paper we have shown that a simple QCD-like model of the dark sector allows for dark pion dark matter that freezes out via semi-annihilation into a dark photon. This is possible due to the existence of a topological interaction between the dark pions χ and the $U(1)_B$ gauge boson X_μ , via the Skyrme current, that is produced by gauging baryon number in the ultraviolet. The model is technically natural, consistent with a range of dark matter mass $10 \text{ MeV} \lesssim m_\chi \lesssim 1 \text{ TeV}$, and evades the limits from indirect detection due to the p -wave nature of the semi-annihilation.

The model has rich phenomenology in cosmology and laboratory experiments. Towards the lighter limit of the allowed mass range, the semi-annihilation process may lead to significant self-interactions that can modify the galactic dynamics at small scales. We discussed potential signatures at colliders, such as monojets at the LHC, invisible Higgs decays at the LHC and at a future Higgs factory, dark spectroscopy at SuperKEKB, and more. We find it intriguing that such a simple model gives rise to a wide ray of rich phenomenology in a way fully consistent with current observational and experimental constraints.

In addition to pursuing more comprehensive phenomenological studies, there are several other future directions we plan to explore. Firstly, it is known that the $2 \rightarrow 1$ process $\chi\chi \rightarrow \chi X$ at the heart of this work can give rise to an alternative DM thermal history besides the freeze-out option explored here, in which the DM abundance starts off very small and is rapidly generated through $X\chi \rightarrow \chi\chi$. This scenario is known as *explosive freeze-in* [75], and it would be interesting to characterise the viable parameter space for this option. Secondly, our restriction to $N_f = 2$ flavours of dark quark can be generalised to $N_f > 2$; in this case, the model also features a WZW term which induces $3 \rightarrow 2$ number changing processes, as has been exploited in theories of Strongly Interacting Massive Particle (SIMP) DM [11, 12]. Including both this WZW term and the gauged baryon number interaction we introduced in this paper, it would be intriguing to study the interplay between the $3\chi \rightarrow 2\chi$ WZW-induced process, which depends on the decay constant f_χ , and the $2\chi \rightarrow \chi X$ semi-annihilation channel, which depends not only on f_χ but also on the gauge coupling e_B .

Acknowledgements

We thank Eric Kuflik, Jesse Thaler, Ayuki Kamada, and Mathias Becker for useful discussions. The work of H. M. is supported by the Director, Office of Science, Office of High Energy Physics of the U.S. Department of Energy under the Contract No. DE-AC02-05CH11231, by the NSF grant PHY-2210390, by the JSPS Grant-in-Aid for Scientific Research JP23K03382, MEXT Grant-in-Aid for Transformative Research Areas (A) JP20H05850, JP20A203, Hamamatsu Photonics, K.K., and Tokyo Dome Corporation. In addition, HM is supported by the World Premier International Research Center Initiative (WPI) MEXT, Japan. Likewise, H. M. thanks the CERN theory group for their warm hospitality during the *Crossroads between Theory and Phenomenology* Program, where this work was initiated. The work of N. S.

has received funding from the INFN Iniziative Specifica APINE. C.S. is supported by the Office of High Energy Physics of the U.S. Department of Energy under contract DE-AC02-05CH11231.

A Semi-Annihilation Computations

In this appendix, we provide details regarding the computation of the thermally-averaged cross-section for the semi-annihilation process. The corresponding matrix-squared element for the process $\chi^a(p_1)\chi^b(p_2) \rightarrow \chi^c(p_3)X^\mu(p_4)$, summed over the final state polarisations and flavours, and averaged over the initial state flavours, is computed using the Feynman rule in Eq. (3.1) and reads

$$\Sigma|\overline{\mathcal{M}}|^2 = \frac{N_f}{N_f^2 - 1} \frac{e_B^2}{64\pi^4 f_\chi^6} (s - 4m_\chi^2) (s - (m_\chi + m_X)^2) (s - (m_\chi - m_X)^2) \sin^2 \theta, \quad (\text{A.1})$$

with the Mandelstam variable s defined as $s = (p_1 + p_2)^2$. In the center-of-mass frame, we have the following momenta configuration when the incoming pions collide along the z -direction and the outgoing photon makes an angle θ with the z -axis in the $y - z$ plane

$$p_1 = \left(\frac{\sqrt{s}}{2}, 0, 0, \frac{\sqrt{s - 4m_\chi^2}}{2} \right), \quad (\text{A.2})$$

$$p_2 = \left(\frac{\sqrt{s}}{2}, 0, 0, -\frac{\sqrt{s - 4m_\chi^2}}{2} \right), \quad (\text{A.3})$$

$$p_3 = \left(\frac{s + m_\chi^2 - m_X^2}{2\sqrt{s}}, 0, |\vec{p}_f| \sin \theta, |\vec{p}_f| \cos \theta \right), \quad (\text{A.4})$$

$$p_4 = \left(\frac{s - m_\chi^2 + m_X^2}{2\sqrt{s}}, 0, -|\vec{p}_f| \sin \theta, -|\vec{p}_f| \cos \theta \right), \quad (\text{A.5})$$

where

$$|\vec{p}_f| = \sqrt{\frac{m_X^4 + (s - m_\chi^2)^2 - 2m_X^2(s + m_\chi^2)}{4s}}. \quad (\text{A.6})$$

The differential cross-section reads

$$\frac{d\sigma_{\chi\chi \rightarrow \chi X}}{d\Omega} = \frac{1}{64\pi^2 s} \frac{|\vec{p}_f|}{|\vec{p}_i|} \Sigma|\overline{\mathcal{M}}|^2, \quad (\text{A.7})$$

with $|\vec{p}_i| = \sqrt{s - 4m_\chi^2}/2$. Now, it is possible to use Eqs. (A.1)–(A.7) and perform the θ -integration with $d\Omega = 2\pi \sin \theta d\theta$ to arrive to

$$\sigma_{\chi\chi \rightarrow \chi X} = \frac{N_f}{N_f^2 - 1} \frac{e_B^2}{1536\pi^5} \frac{(m_X^4 + (s - m_\chi^2)^2 - 2m_X^2(s + m_\chi^2))^{3/2}}{f_\chi^6 s^{3/2}}, \quad (\text{A.8})$$

which, in the limit $m_\chi \rightarrow 0$

$$\sigma_{\chi\chi \rightarrow \chi X} = \frac{N_f}{N_f^2 - 1} \frac{e_B^2}{1536\pi^5} \frac{s^2}{f_\chi^6} \left(1 - \frac{m_\chi^2}{s}\right)^3 \left(1 - \frac{4m_\chi^2}{s}\right)^{1/2}, \quad (\text{A.9})$$

reproduces Eq. (3.2) from the main text. Following Refs. [40, 41], we compute the thermally averaged cross section times the Møller velocity, $v = \sqrt{|\mathbf{v}_1 - \mathbf{v}_2|^2 - |\mathbf{v}_1 \times \mathbf{v}_2|^2}$, as the following integral

$$\langle \sigma v \rangle_{\chi\chi \rightarrow \chi X} = \frac{\int_{4m_\chi^2}^{\infty} \sigma_{\chi\chi \rightarrow \chi X} \sqrt{s} (s - 4m_\chi^2) K_1(\sqrt{s}/T) ds}{8m_\chi^4 T K_2^2(m_\chi/T)}, \quad (\text{A.10})$$

with K_i being the modified Bessel functions of the i -th order. Solving the integral, we find

$$\begin{aligned} \langle \sigma v \rangle_{\chi\chi \rightarrow \chi X} = & \frac{N_f}{N_f^2 - 1} \frac{e_B^2}{4096\pi^{9/2}} \frac{m_\chi^4}{f_\chi^6} \frac{x}{K_2^2(x)} \left[64 G_{1,3}^{3,0} \left(-\frac{9}{2} - \frac{1}{2} \frac{1}{2} \middle| x^2 \right) - 48 G_{1,3}^{3,0} \left(-\frac{7}{2} - \frac{1}{2} \frac{1}{2} \middle| x^2 \right) \right. \\ & \left. + 12 G_{1,3}^{3,0} \left(-\frac{5}{2} - \frac{1}{2} \frac{1}{2} \middle| x^2 \right) - G_{1,3}^{3,0} \left(-\frac{3}{2} - \frac{1}{2} \frac{1}{2} \middle| x^2 \right) \right], \end{aligned} \quad (\text{A.11})$$

where $x = m_\chi/T$, and $G(x^2)$ is the Meijer G-function [42].

The expression for $\langle \sigma v \rangle_{\chi\chi \rightarrow \chi X}$ can be expanded in the inverse powers of $x = m_\chi/T$. Up to $\mathcal{O}(x^{-3})$, the corresponding expression reads

$$\langle \sigma v \rangle_{\chi\chi \rightarrow \chi X} = \frac{N_f}{N_f^2 - 1} \frac{e_B^2}{384\pi^5} \frac{m_\chi^4}{f_\chi^6} \left(\frac{81}{16} x^{-1} + \frac{891}{32} x^{-2} - \frac{66825}{512} x^{-3} + \dots \right). \quad (\text{A.12})$$

Furthermore, it correctly reproduces the result in the non-relativistic limit, $x \gg 1$. Indeed, starting from Eq. (3.2), the non-relativistic limit of the thermally averaged cross-section is

$$\langle \sigma v \rangle_{\chi\chi \rightarrow \chi X}^{\text{nr}} = \left\langle \sigma_{\chi\chi \rightarrow \chi X} \cdot 2\sqrt{1 - 4m_\chi^2/s} \right\rangle, \quad (\text{A.13})$$

with $s = 4m_\chi^2 + m_\chi^2 v^2$. Therefore, expanding the right-hand side of Eq. (A.13) in v^2 and using

$$\langle v^n \rangle = \frac{2^{(n-1)/2} \Gamma(\frac{n+3}{2})}{\Gamma(\frac{3}{2})} x^{-n/2}, \quad (\text{A.14})$$

we find

$$\langle \sigma v \rangle_{\chi\chi \rightarrow \chi X}^{\text{nr}} = \frac{N_f}{N_f^2 - 1} \frac{e_B^2}{384\pi^5} \frac{m_\chi^4}{f_\chi^6} \left(\frac{81}{16} x^{-1} + \frac{405}{128} x^{-2} + \frac{945}{2048} x^{-3} + \dots \right), \quad (\text{A.15})$$

with the leading term matching the one in Eq. (A.12).

B Annihilation Computations

The operators in the chiral Lagrangian can mediate the $\chi^a(p_1)\chi^b(p_2) \rightarrow X^\mu(p_3)X^\nu(p_4)$ process. There are two independent dimension-six operators, as given also in the main text,

$$\mathcal{L}_{\chi\text{PT}} \supset \left(\frac{e_B}{16\pi^2 f_\chi} \right)^2 \left(\lambda_1 \left(\partial_\alpha U^\dagger \right) (\partial^\alpha U) X_{\mu\nu} X^{\mu\nu} + \lambda_2 \left(\partial_\alpha U^\dagger \right) (\partial^\nu U) X_{\mu\nu} X^{\mu\alpha} \right), \quad (\text{B.1})$$

where λ_1 and λ_2 are $\mathcal{O}(1)$ Wilson coefficients (in general complex), and the overall size is set by the dimensionful factor in front. The corresponding Feynman rules read

$$\mathcal{O}_1 : -8i\lambda_1 p_3 \cdot p_4 (p_4^\mu p_3^\nu - p_3 \cdot p_4 g^{\mu\nu}) \delta^{ab}, \quad (\text{B.2})$$

$$\begin{aligned} \mathcal{O}_2 : & 2i\lambda_2 (p_1 \cdot p_4 p_2^\mu p_3^\nu + p_1 \cdot p_3 p_4^\mu p_2^\nu - p_3 \cdot p_4 (p_1^\mu p_2^\nu + p_2^\mu p_1^\nu) \\ & + p_2 \cdot p_4 (p_1^\mu p_3^\nu - p_1 \cdot p_3 g^{\mu\nu}) + p_2 \cdot p_3 (p_4^\mu p_1^\nu - p_1 \cdot p_4 g^{\mu\nu})) \delta^{ab}, \end{aligned} \quad (\text{B.3})$$

multiplied by the overall size of the UV contribution, $(e_B/16\pi^2 f_\chi)^2$.

We can use this to compute the thermally averaged cross section as outlined in Sec. 3.1. The result for the averaged matrix element squared reads

$$\begin{aligned} \sum |\overline{\mathcal{M}}|^2 = & \frac{1}{N_f^2 - 1} \left(\frac{e_B}{16\pi^2 f_\chi^2} \right)^4 \left[4s^2 (s - 2m_\chi^2)^2 (\text{Re}(\lambda_1 \lambda_2^*) + 2|\lambda_1|^2) \right. \\ & \left. + \left(2m_\chi^4 s^2 + \frac{1}{2}s^2 (s - 2m_\chi^2)^2 - 4m_\chi^2 s (t - m_\chi^2)(u - m_\chi^2) + 2(t - m_\chi^2)^2 (u - m_\chi^2)^2 \right) |\lambda_2|^2 \right]. \end{aligned} \quad (\text{B.4})$$

The corresponding cross-section is

$$\begin{aligned} \sigma_{\chi\chi \rightarrow XX} = & \frac{1}{N_f^2 - 1} \left(\frac{e_B}{16\pi^2 f_\chi^2} \right)^4 \frac{1}{4\pi} s \sqrt{\frac{s}{s - 4m_\chi^2}} \\ & \times \left[(s - 2m_\chi^2)^2 (\text{Re}(\lambda_1 \lambda_2^*) + 2|\lambda_1|^2) - \frac{1}{120} (92m_\chi^4 - 76m_\chi^2 s + 17s^2) |\lambda_2|^2 \right], \end{aligned} \quad (\text{B.5})$$

and the thermally averaged cross-section

$$\begin{aligned} \langle \sigma v \rangle_{\chi\chi \rightarrow XX} = & \frac{1}{N_f^2 - 1} \left(\frac{e_B}{16\pi^2 f_\chi^2} \right)^4 \frac{16m_\chi^6}{\sqrt{\pi}} \frac{x}{K_2^2(x)} \\ & \left[G_{1,3}^{3,0} \left(-\frac{4}{-\frac{11}{2} - \frac{1}{2} \frac{1}{2}} |x^2 \right) \left(\text{Re}(\lambda_1 \lambda_2^*) + 2|\lambda_1|^2 + \frac{17}{2} |\lambda_2|^2 \right) \right. \\ & - G_{1,3}^{3,0} \left(-\frac{3}{-\frac{9}{2} - \frac{1}{2} \frac{1}{2}} |x^2 \right) \left(\text{Re}(\lambda_1 \lambda_2^*) + 2|\lambda_1|^2 + \frac{19}{2} |\lambda_2|^2 \right) \\ & \left. + \frac{1}{4} G_{1,3}^{3,0} \left(-\frac{2}{-\frac{7}{2} - \frac{1}{2} \frac{1}{2}} |x^2 \right) \left(\text{Re}(\lambda_1 \lambda_2^*) + 2|\lambda_1|^2 + \frac{23}{2} |\lambda_2|^2 \right) \right]. \end{aligned} \quad (\text{B.6})$$

Expanding $\langle \sigma v \rangle_{\chi\chi \rightarrow XX}$ in the limit of large x , we obtain

$$\langle \sigma v \rangle_{\chi\chi \rightarrow XX} \approx \frac{1}{N_f^2 - 1} \left(\frac{e_B}{16\pi^2 f_\chi^2} \right)^4 \frac{m_\chi^6}{\pi} |4\lambda_1 + \lambda_2|^2 \left(1 + \frac{15}{8} x^{-1} + \mathcal{O}(x^{-2}) \right). \quad (\text{B.7})$$

C Semi-Analytical *vs.* Numerical Results

In this appendix, we compare the numerical results for x_f (the freeze-out moment) and $Y_\chi(x_\infty)$ (the asymptotic limit of the dark pion yield today, $x \rightarrow x_\infty$) with the semi-analytic solutions that we present below.

We first solve for x_f in Eq (4.12) in the non-relativistic limit, keeping only the leading order in x^{-1} from each cross-section. For later convenience, we write the cross-sections as $\langle \sigma v \rangle_{\chi\chi \rightarrow XX} \approx \sigma_a x^{-n_a}$ and $\langle \sigma v \rangle_{\chi\chi \rightarrow \chi X} \approx \sigma_s x^{-n_s}$, where n_i denotes the leading power in the x^{-1} expansion ($n_a = 0$ for s -wave annihilations, and $n_s = 1$ for p -wave semi-annihilations). Therefore, we have

$$x_f \simeq \log \left[c(c+1) 0.0382 \frac{M_{\text{Pl}} m_\chi \sigma_s}{\sqrt{g_*}} \right] - \left[n_s + \frac{1}{2} \right] \log[x_f] + \log \left[1 + \frac{\sigma_a}{\sigma_s} \frac{c+2}{c+1} x_f \right]. \quad (\text{C.1})$$

For annihilation processes, the best fit for c is to choose $c(c+2) = n_a + 1$ [76]. Since semi-annihilation is the dominant process here, we choose $c(c+1) = n_s + 1$. For our p -wave process $c = 1$.

$$x_f \simeq \log \left[c(c+1) 0.0382 \frac{M_{\text{Pl}} m_\chi \sigma_s}{\sqrt{g_*}} \right] - \left[c(c+1) - \frac{1}{2} \right] \log[x_f] + \log \left[1 + \frac{\sigma_a}{\sigma_s} \frac{c+2}{c+1} x_f \right]. \quad (\text{C.2})$$

Moreover, we can use that $\frac{\sigma_a}{\sigma_s} \sim \frac{4}{3(16\pi^2)^2} \frac{m_\chi^2 e_B^2}{f_\chi^2 N_f}$, with x_f of order 10, and for the choices of m_χ and f_χ considered, the last log in the expression above is subleading. In this case, we find

$$x_f \simeq \ln \left[0.038 c(c+1) \frac{1}{g_*^{1/2}} M_{\text{Pl}} m_\chi \sigma_s \right] - \left(c(c+1) - \frac{1}{2} \right) \ln \left\{ \ln \left[0.038 c(c+1) \frac{1}{g_*^{1/2}} M_{\text{Pl}} m_\chi \sigma_s \right] \right\} \\ + \ln \left\{ 1 + \frac{\sigma_a}{\sigma_s} \frac{(c+2)}{(c+1)} \ln \left(0.038 \frac{1}{g_*^{1/2}} M_{\text{Pl}} m_\chi \sigma_s \right) \right\}, \quad (\text{C.3})$$

and

$$Y_\infty \simeq \frac{3.79 g_*^{1/2}}{M_{\text{Pl}} m_\chi (\sigma_a x_f^{-1} + \frac{1}{2} \sigma_s x_f^{-2})}. \quad (\text{C.4})$$

The results and their comparison to the fully numerical solutions for a couple of benchmark values of the parameters are shown in the tables below.

$\mathbf{N_f = 2, e_B = 1, \lambda_1 = 1, \lambda_2 = 1, c = 1}$:

f_χ [GeV]	m_χ [GeV]	g_*	x_f	Y_∞	Y(50) (numeric)	Y(75) (numeric)
5	2.8	247/4	20.21	$5.10 \cdot 10^{-11}$	$5.17 \cdot 10^{-11}$	$4.69 \cdot 10^{-11}$
50	94	303/4	23.66	$1.46 \cdot 10^{-12}$	$1.64 \cdot 10^{-12}$	$1.43 \cdot 10^{-12}$
500	3175	345/4	27.32	$3.62 \cdot 10^{-14}$	$5.10 \cdot 10^{-14}$	$4.17 \cdot 10^{-14}$

$$\mathbf{N_f} = \mathbf{2}, \mathbf{e_B} = \mathbf{0.01}, \lambda_1 = \mathbf{1}, \lambda_2 = \mathbf{1}, \mathbf{c} = \mathbf{1} :$$

f_χ [GeV]	m_χ [GeV]	g_*	x_f	Y_∞	Y(50) (numeric)	Y(75) (numeric)
5	2.8	247/4	11.68	$1.71 \cdot 10^{-7}$	$1.43 \cdot 10^{-7}$	$1.39 \cdot 10^{-7}$
50	94	303/4	15.02	$5.97 \cdot 10^{-9}$	$5.38 \cdot 10^{-9}$	$5.13 \cdot 10^{-9}$
500	3175	345/4	18.48	$1.93 \cdot 10^{-10}$	$1.86 \cdot 10^{-10}$	$1.72 \cdot 10^{-10}$

References

- [1] M. Cirelli, A. Strumia, and J. Zupan, “*Dark Matter*,” [arXiv:2406.01705](#).
- [2] Y. Bai and P. Schwaller, “*Scale of dark QCD*,” *Phys. Rev. D* **89** (2014) no. 6, 063522, [arXiv:1306.4676](#).
- [3] G. D. Kribs and E. T. Neil, “*Review of strongly-coupled composite dark matter models and lattice simulations*,” *Int. J. Mod. Phys. A* **31** (2016) no. 22, 1643004, [arXiv:1604.04627](#).
- [4] B. Holdom, “*Two $U(1)$ ’s and Epsilon Charge Shifts*,” *Phys. Lett. B* **166** (1986) 196–198.
- [5] B. Patt and F. Wilczek, “*Higgs-field portal into hidden sectors*,” [arXiv:hep-ph/0605188](#).
- [6] A. Falkowski, J. Juknevič, and J. Shelton, “*Dark Matter Through the Neutrino Portal*,” [arXiv:0908.1790](#).
- [7] T. H. R. Skyrme, “*A Nonlinear field theory*,” *Proc. Roy. Soc. Lond. A* **260** (1961) 127–138.
- [8] J. Goldstone and F. Wilczek, “*Fractional Quantum Numbers on Solitons*,” *Phys. Rev. Lett.* **47** (1981) 986–989.
- [9] A. P. Balachandran, V. P. Nair, S. G. Rajeev, and A. Stern, “*Exotic Levels from Topology in the QCD Effective Lagrangian*,” *Phys. Rev. Lett.* **49** (1982) 1124. [Erratum: *Phys.Rev.Lett.* 50, 1630 (1983)].
- [10] E. Witten, “*Current Algebra, Baryons, and Quark Confinement*,” *Nucl. Phys. B* **223** (1983) 433–444.
- [11] Y. Hochberg, E. Kuflik, T. Volansky, and J. G. Wacker, “*Mechanism for Thermal Relic Dark Matter of Strongly Interacting Massive Particles*,” *Phys. Rev. Lett.* **113** (2014) 171301, [arXiv:1402.5143](#).
- [12] Y. Hochberg, E. Kuflik, H. Murayama, T. Volansky, and J. G. Wacker, “*Model for Thermal Relic Dark Matter of Strongly Interacting Massive Particles*,” *Phys. Rev. Lett.* **115** (2015) no. 2, 021301, [arXiv:1411.3727](#).
- [13] J. Davighi, A. Greljo, and N. Selimovic, “*Topological Portal to the Dark Sector*,” *Phys. Rev. Lett.* **134** (2025) no. 11, 111804, [arXiv:2401.09528](#).
- [14] J. Davighi and N. Lohitsiri, “*WZW terms without anomalies: Generalised symmetries in chiral Lagrangians*,” *SciPost Phys.* **17** (2024) no. 6, 168, [arXiv:2407.20340](#).
- [15] J. Wess and B. Zumino, “*Consequences of anomalous Ward identities*,” *Phys. Lett. B* **37** (1971) 95–97.
- [16] E. Witten, “*Global Aspects of Current Algebra*,” *Nucl. Phys. B* **223** (1983) 422–432.

- [17] F. D’Eramo and J. Thaler, “*Semi-annihilation of Dark Matter*,” *JHEP* **06** (2010) 109, [arXiv:1003.5912](#).
- [18] T. Hambye, “*Hidden vector dark matter*,” *JHEP* **01** (2009) 028, [arXiv:0811.0172](#).
- [19] E. D. Kramer, E. Kuflik, N. Levi, N. J. Outmezguine, and J. T. Ruderman, “*Heavy Thermal Dark Matter from a New Collision Mechanism*,” *Phys. Rev. Lett.* **126** (2021) no. 8, 081802, [arXiv:2003.04900](#).
- [20] A. Kamada, M. Kaplinghat, A. B. Pace, and H.-B. Yu, “*How the Self-Interacting Dark Matter Model Explains the Diverse Galactic Rotation Curves*,” *Phys. Rev. Lett.* **119** (2017) no. 11, 111102, [arXiv:1611.02716](#).
- [21] M. Rocha, A. H. G. Peter, J. S. Bullock, M. Kaplinghat, S. Garrison-Kimmel, J. Onorbe, and L. A. Moustakas, “*Cosmological Simulations with Self-Interacting Dark Matter I: Constant Density Cores and Substructure*,” *Mon. Not. Roy. Astron. Soc.* **430** (2013) 81–104, [arXiv:1208.3025](#).
- [22] A. H. G. Peter, M. Rocha, J. S. Bullock, and M. Kaplinghat, “*Cosmological Simulations with Self-Interacting Dark Matter II: Halo Shapes vs. Observations*,” *Mon. Not. Roy. Astron. Soc.* **430** (2013) 105, [arXiv:1208.3026](#).
- [23] R. A. Flores and J. R. Primack, “*Observational and theoretical constraints on singular dark matter halos*,” *Astrophys. J. Lett.* **427** (1994) L1–4, [arXiv:astro-ph/9402004](#).
- [24] J. F. Navarro, C. S. Frenk, and S. D. M. White, “*The Structure of cold dark matter halos*,” *Astrophys. J.* **462** (1996) 563–575, [arXiv:astro-ph/9508025](#).
- [25] B. Moore, T. R. Quinn, F. Governato, J. Stadel, and G. Lake, “*Cold collapse and the core catastrophe*,” *Mon. Not. Roy. Astron. Soc.* **310** (1999) 1147–1152, [arXiv:astro-ph/9903164](#).
- [26] B. Moore, S. Ghigna, F. Governato, G. Lake, T. R. Quinn, J. Stadel, and P. Tozzi, “*Dark matter substructure within galactic halos*,” *Astrophys. J. Lett.* **524** (1999) L19–L22, [arXiv:astro-ph/9907411](#).
- [27] A. A. Klypin, A. V. Kravtsov, O. Valenzuela, and F. Prada, “*Where are the missing Galactic satellites?*,” *Astrophys. J.* **522** (1999) 82–92, [arXiv:astro-ph/9901240](#).
- [28] M. Boylan-Kolchin, J. S. Bullock, and M. Kaplinghat, “*Too big to fail? The puzzling darkness of massive Milky Way subhaloes*,” *Mon. Not. Roy. Astron. Soc.* **415** (2011) L40, [arXiv:1103.0007](#).
- [29] M. Boylan-Kolchin, J. S. Bullock, and M. Kaplinghat, “*The Milky Way’s bright satellites as an apparent failure of Λ CDM*,” *Mon. Not. Roy. Astron. Soc.* **422** (2012) 1203–1218, [arXiv:1111.2048](#).
- [30] K. A. Oman *et al.*, “*The unexpected diversity of dwarf galaxy rotation curves*,” *Mon. Not. Roy. Astron. Soc.* **452** (2015) no. 4, 3650–3665, [arXiv:1504.01437](#).
- [31] M. Kawasaki, H. Nakatsuka, K. Nakayama, and T. Sekiguchi, “*Revisiting CMB constraints on dark matter annihilation*,” *JCAP* **12** (2021) no. 12, 015, [arXiv:2105.08334](#).
- [32] K. N. Abazajian, S. Horiuchi, M. Kaplinghat, R. E. Keeley, and O. Macias, “*Strong constraints on thermal relic dark matter from Fermi-LAT observations of the Galactic Center*,” *Phys. Rev. D* **102** (2020) no. 4, 043012, [arXiv:2003.10416](#).

- [33] G. 't Hooft, “*Naturalness, chiral symmetry, and spontaneous chiral symmetry breaking*,” *NATO Sci. Ser. B* **59** (1980) 135–157.
- [34] M. Reece, “*TASI Lectures: (No) Global Symmetries to Axion Physics*,” *PoS TASI2022* (2024) 008, [arXiv:2304.08512](#).
- [35] L. J. Hall and H. Murayama, “*A Geometry of the generations*,” *Phys. Rev. Lett.* **75** (1995) 3985–3988, [arXiv:hep-ph/9508296](#).
- [36] D. Gaiotto, A. Kapustin, N. Seiberg, and B. Willett, “*Generalized Global Symmetries*,” *JHEP* **02** (2015) 172, [arXiv:1412.5148](#).
- [37] A. Kapustin and R. Thorngren, “*Higher Symmetry and Gapped Phases of Gauge Theories*,” *Prog. Math.* **324** (2017) 177–202, [arXiv:1309.4721](#).
- [38] C. Córdova, T. T. Dumitrescu, and K. Intriligator, “*Exploring 2-Group Global Symmetries*,” *JHEP* **02** (2019) 184, [arXiv:1802.04790](#).
- [39] C. Córdova, T. T. Dumitrescu, and K. Intriligator, “*2-Group Global Symmetries and Anomalies in Six-Dimensional Quantum Field Theories*,” *JHEP* **04** (2021) 252, [arXiv:2009.00138](#).
- [40] P. Gondolo and G. Gelmini, “*Cosmic abundances of stable particles: Improved analysis*,” *Nucl. Phys. B* **360** (1991) 145–179.
- [41] J. Edsjö and P. Gondolo, “*Neutralino relic density including coannihilations*,” *Phys. Rev. D* **56** (1997) 1879–1894, [arXiv:hep-ph/9704361](#).
- [42] V. Adamchik, “*The evaluation of integrals of Bessel functions via G-function identities*,” *Journal of Computational and Applied Mathematics* **64** (1995) no. 3, 283–290. <https://www.sciencedirect.com/science/article/pii/0377042795001530>.
- [43] **Planck**, N. Aghanim *et al.*, “*Planck 2018 results. VI. Cosmological parameters*,” *Astron. Astrophys.* **641** (2020) A6, [arXiv:1807.06209](#). [Erratum: *Astron. Astrophys.* 652, C4 (2021)].
- [44] A. Kamada, H. J. Kim, H. Kim, and T. Sekiguchi, “*Self-Heating Dark Matter via Semiannihilation*,” *Phys. Rev. Lett.* **120** (2018) no. 13, 131802, [arXiv:1707.09238](#).
- [45] A. Kamada, H. J. Kim, J.-C. Park, and S. Shin, “*Manifesting hidden dynamics of a sub-component dark matter*,” *JCAP* **10** (2022) 052, [arXiv:2111.06808](#).
- [46] K. M. Nollett and G. Steigman, “*BBN And The CMB Constrain Light, Electromagnetically Coupled WIMPs*,” *Phys. Rev. D* **89** (2014) no. 8, 083508, [arXiv:1312.5725](#).
- [47] X. Chu, C. Garcia-Cely, and H. Murayama, “*Velocity Dependence from Resonant Self-Interacting Dark Matter*,” *Phys. Rev. Lett.* **122** (2019) no. 7, 071103, [arXiv:1810.04709](#).
- [48] Y.-D. Tsai, R. McGehee, and H. Murayama, “*Resonant Self-Interacting Dark Matter from Dark QCD*,” *Phys. Rev. Lett.* **128** (2022) no. 17, 172001, [arXiv:2008.08608](#).
- [49] D. Kondo, R. McGehee, T. Melia, and H. Murayama, “*Linear sigma dark matter*,” *JHEP* **09** (2022) 041, [arXiv:2205.08088](#).
- [50] S. Ando, K. Hayashi, S. Horigome, M. Ibe, and S. Shirai, “*Stringent Constraints on Self-Interacting Dark Matter Using Milky-Way Satellite Galaxies Kinematics*,” [arXiv:2503.13650](#).

- [51] A. Caputo, A. J. Millar, C. A. J. O’Hare, and E. Vitagliano, “Dark photon limits: A handbook,” *Phys. Rev. D* **104** (2021) no. 9, 095029, [arXiv:2105.04565](#).
- [52] **ATLAS**, G. Aad *et al.*, “Search for dark matter in association with an energetic photon in pp collisions at $\sqrt{s} = 13$ TeV with the ATLAS detector,” *JHEP* **02** (2021) 226, [arXiv:2011.05259](#).
- [53] **ATLAS**, “Search for high-mass resonances in photon plus missing transverse momentum signatures in pp collisions at $\sqrt{s} = 13$ TeV with the ATLAS detector,”.
- [54] **ATLAS**, “Prospects for Dark Matter searches in mono-photon and $VBF+E_T^{miss}$ final states in ATLAS,”.
- [55] T. Han, Z. Liu, L.-T. Wang, and X. Wang, “WIMPs at High Energy Muon Colliders,” *Phys. Rev. D* **103** (2021) no. 7, 075004, [arXiv:2009.11287](#).
- [56] **BaBar**, J. P. Lees *et al.*, “Search for Invisible Decays of a Dark Photon Produced in e^+e^- Collisions at BaBar,” *Phys. Rev. Lett.* **119** (2017) no. 13, 131804, [arXiv:1702.03327](#).
- [57] **Belle-II**, W. Altmannshofer *et al.*, “The Belle II Physics Book,” *PTEP* **2019** (2019) no. 12, 123C01, [arXiv:1808.10567](#). [Erratum: *PTEP* 2020, 029201 (2020)].
- [58] Y. Hochberg, E. Kuflik, and H. Murayama, “SIMP Spectroscopy,” *JHEP* **05** (2016) 090, [arXiv:1512.07917](#).
- [59] Y. Hochberg, E. Kuflik, and H. Murayama, “Dark spectroscopy at lepton colliders,” *Phys. Rev. D* **97** (2018) no. 5, 055030, [arXiv:1706.05008](#).
- [60] **CMS**, A. M. Sirunyan *et al.*, “Search for dark photons in Higgs boson production via vector boson fusion in proton-proton collisions at $\sqrt{s} = 13$ TeV,” *JHEP* **03** (2021) 011, [arXiv:2009.14009](#).
- [61] **ATLAS**, G. Aad *et al.*, “Search for dark photons from Higgs boson decays via ZH production with a photon plus missing transverse momentum signature from pp collisions at $\sqrt{s} = 13$ TeV with the ATLAS detector,” *JHEP* **07** (2023) 133, [arXiv:2212.09649](#).
- [62] **Particle Data Group**, S. Navas *et al.*, “Review of particle physics,” *Phys. Rev. D* **110** (2024) no. 3, 030001.
- [63] M. E. Peskin, “Estimation of LHC and ILC Capabilities for Precision Higgs Boson Coupling Measurements,” in *Snowmass 2013: Snowmass on the Mississippi*. 12, 2013. [arXiv:1312.4974](#).
- [64] Z. Liu, L.-T. Wang, and H. Zhang, “Exotic decays of the 125 GeV Higgs boson at future e^+e^- lepton colliders,” *Chin. Phys. C* **41** (2017) no. 6, 063102, [arXiv:1612.09284](#).
- [65] S. Dawson *et al.*, “Report of the Topical Group on Higgs Physics for Snowmass 2021: The Case for Precision Higgs Physics,” in *Snowmass 2021*. 9, 2022. [arXiv:2209.07510](#).
- [66] **ATLAS**, M. Aaboud *et al.*, “Search for new phenomena in final states with an energetic jet and large missing transverse momentum in pp collisions at $\sqrt{s} = 13$ TeV using the ATLAS detector,” *Phys. Rev. D* **94** (2016) no. 3, 032005, [arXiv:1604.07773](#).
- [67] **CMS**, A. Tumasyan *et al.*, “Search for new particles in events with energetic jets and large missing transverse momentum in proton-proton collisions at $\sqrt{s} = 13$ TeV,” *JHEP* **11** (2021) 153, [arXiv:2107.13021](#).
- [68] A. Boveia *et al.*, “Summarizing experimental sensitivities of collider experiments to dark matter models and comparison to other experiments,” [arXiv:2206.03456](#).

- [69] **CMS**, A. M. Sirunyan *et al.*, “Search for a Narrow Resonance Lighter than 200 GeV Decaying to a Pair of Muons in Proton-Proton Collisions at $\sqrt{s} = \text{TeV}$,” *Phys. Rev. Lett.* **124** (2020) no. 13, 131802, [arXiv:1912.04776](#).
- [70] **CMS**, A. Tumasyan *et al.*, “Search for low-mass dilepton resonances in Higgs boson decays to four-lepton final states in proton-proton collisions at $\sqrt{s} = 13 \text{ TeV}$,” *Eur. Phys. J. C* **82** (2022) no. 4, 290, [arXiv:2111.01299](#).
- [71] D. Curtin, R. Essig, S. Gori, and J. Shelton, “Illuminating Dark Photons with High-Energy Colliders,” *JHEP* **02** (2015) 157, [arXiv:1412.0018](#).
- [72] M. He, X.-G. He, C.-K. Huang, and G. Li, “Search for a heavy dark photon at future e^+e^- colliders,” *JHEP* **03** (2018) 139, [arXiv:1712.09095](#).
- [73] T. Cohen, M. Lisanti, and H. K. Lou, “Semivisible Jets: Dark Matter Undercover at the LHC,” *Phys. Rev. Lett.* **115** (2015) no. 17, 171804, [arXiv:1503.00009](#).
- [74] M. Buschmann, J. Kopp, J. Liu, and P. A. N. Machado, “Lepton Jets from Radiating Dark Matter,” *JHEP* **07** (2015) 045, [arXiv:1505.07459](#).
- [75] T. Bringmann, P. F. Depta, M. Hufnagel, J. T. Ruderman, and K. Schmidt-Hoberg, “Dark Matter from Exponential Growth,” *Phys. Rev. Lett.* **127** (2021) no. 19, 191802, [arXiv:2103.16572](#).
- [76] E. W. Kolb and M. S. Turner, *The early universe*. CRC Press, Taylor et Francis Group, 2018.